TAMPERE UNIVERSITY OF TECHNOLOGY

MANOJ SIVASUBRAMANIAPANDIAN

THE EFFECT OF COATINGS ON THE PERFORMANCE OF THE MICROELECTRODE ARRAYS

Master of Science Thesis

Examiners:
Professor Jukka Lekkala
MSc. Tomi Ryynänen

Examiners and topic approved at the council meeting of the Faculty of Natural Sciences on February 06, 2013.

ABSTRACT

TAMPERE UNIVERSITY OF TECHNOLOGY
Master's Degree Programme in Biomedical Engineering
MANOJ SIVASUBRAMANIAPANDIAN: The Effect of Coatings on the Performance of the Microelectrode Arrays
Master of Science Thesis, 77 pages, 3 appendix pages
December 2013
Major: Medical Instrumentation
Examiners: Professor Jukka Lekkala, MSc. Tomi Ryynänen
Keywords: Coating materials, impedance, kinetics of adsorption, microelectrode arrays, noise, surface characterisation.

Microelectrode arrays (MEAs) are pretreated with suitable surface molecules prior to culturing of cells, since the properties of the substrate have a decisive effect on the adhesion, migration, differentiation, and the growth of the cells. The purpose of this thesis is to study a few of these coating materials, and to evaluate their impact on the performance of the MEA.

Standard 8×8 MEA is used alongside the 6 well MEAs, and the differences in the impedances and the noise magnitudes of the electrodes are analysed upon coating. Experiments with neural cells were conducted in order to realise the repercussions on real life applications. An effort is also made to determine the thickness and the surface texture of the coatings, using a stylus profilometer and an atomic force microscope (AFM) respectively.

Polyethyleneimine (PEI) and laminin, and gelatin coatings did not effect any significant change in the overall performance of the MEAs, but a substantial increase in impedance was observed with Matrigel^{TM}. The experiments involving the cells were inconclusive due to limitations in imaging. The thickness measurements of the PEI and laminin, and gelatin coatings were unsuccessful, owing to the intrinsic surface variations of the substrate. However, the thickness of the Matrigel^{TM} coating was found to increase with the concentration. Surface characterisation of the MEAs revealed significant variations in the surface roughness, with the addition of PEI and laminin. The kinetics of adsorption of the PEI and laminin molecules to the sensor slide was studied using surface plasmon resonance (SPR).

PREFACE

This Master of Science Thesis was conducted at the Department of Automation Science and Engineering, Tampere University of Technology, as part of the Human Spare Parts research program, jointly funded by TEKES, Academy of Finland, The Council of Tampere Region, the European Union and its frontier-sciences arm, and the European Research Council. The work was carried out in association with two other research groups from the Institute of Biomedical Technology, University of Tampere, the Neuro group, and the Heart group.

The PDMS structures for the MEAs were provided by Joose Kreutzer from the Department of Automation Science and Engineering. Tomi Ryynänen from the same department was responsible for the surface characterization of the MEAs using the AFM. The experiments with the cells, involving cell plating and fluorescence imaging were performed by Marja Pajunen from the Neuro group.

I would like to express my gratitude to my examiners, Professor Jukka Lekkala, and MSc. Tomi Ryynänen for their guidance during the study. I also thank Janne Koivisto from the Heart group, and Marja Pajunen for sharing their insights, and assisting with the MEA coatings. I would like to gratefully acknowledge Jouni Niemelä and Juha Heikkilä for their technical assistance during the course of my work. My heart felt appreciation to the staff at both the Department of Automation Science and Engineering, and the Institute of Biomedical Technology for providing a conducive environment to work.

Finally, my family and friends. Thank you for all the sacrifices you have made, and the endless love and support.

Tampere, February 19, 2014

Manoj Sivasubramaniapandian
Insinöörinkatu 60 B 100
33720 Tampere

TABLE OF CONTENTS

ABBREVIATIONS AND NOTATION

AFM	Atomic force microscope
BNC	Bayonet Neill-Concelman
CE	Counter electrode
DC-37	D-subminiatures with 37 contact pins
DMEM	Dulbecco's modified eagle medium
IHP	Inner Helmholtz plane
MEA	Microelectrode array
NDM	Neural differentiation medium
OHP	Outer Helmholtz plane
PBS	Phosphate buffered saline
PDMS	Polydimethylsiloxane
PEI	Polyethyleneimine
RE	Reference electrode
SCSI	Small computer system interface
SNR	Signal-to-noise ratio
USB	Universal serial bus
WE	Working electrode
c_A	Concentration of ions 'A' in the solution
C_{es}	Equivalent capacitance of the electrode-electrolyte interface
$C_{es,s}$	Equivalent electrode capacitance within the seal area
C_G	Gouy-Chapman capacitance
C_H	Helmholz capacitance
C_I	Interface capacitance
C_{in}	Input capacitance
C_m	Capacitance of the cell membrane
$C_{m,s}$	Collective membrane capacitance within the seal area
C_p	Parasitic capacitance
D_i	Diffusion coefficient of the ion
d_{OHP}	Thickness of the electric double layer
F	Faraday's constant
$i_{n,rs}$	Noise current at R_S
$i_{n,res}$	Noise current at R_{es}
i_{sig}	Ionic current from the cell
$i(t)$	Time varying current
J_o	Equilibrium exchange current density
k	Boltzmann's constant
k_c	Rate constant of the reduction reaction

k_{eff}	Shift in spring constant
k_n	Free space wave number
k_o	Intrinsic spring constant
L	Sample length
L_D	Debye length
n	Empirical factor representing the surface inhomogeneities
n_1	Number of samples
n^o	Bulk number concentration of ions in the solution
n_s	Refractive index of the dielectric
q	Elementary charge
r	Radius of the electrode
R	Gas constant
R_a	Arithmetic average deviation from the mean
R_{ct}	Charge transfer resistance
R_{es}	Equivalent resistance of the electrode-electrolyte interface
R_m	Resistance of the cell membrane
$R_{m,s}$	Collective membrane resistance with the seal area
R_p	Maximum peak height from the mean
R_{pm}	Average peak-to-mean height
R_q	RMS value of surface roughness
R_r	Resistance of the routing path
R_s	Solution resistance
R_S	Seal resistance
R_v	Maximum valley depth from the mean
R_z	Average peak-to-valley height
T	Temperature
U_c^*	Compensation voltage
U_s^*	Sample voltage
U_t	Thermal voltage
V_0	Applied voltage
V_{rms}	RMS noise voltage
$V_{n,in,res}$	Magnitude of R_{es} noise at the amplifier input
$V_{n,in,rs}$	Magnitude of R_S noise at the amplifier input
$V(t)$	Time varying voltage signal
x_i	Noise amplitude at the instant i
Z	Ionic charge of the solution
Z_{CPA}	Constant phase angle impedance
Z_s^*	Sample impedance
Z_c^*	Compensation impedance

z_i	Charge of the ion
Z_w	Warburg impedance
$Z(x)$	Profile height measured from the reference line
β	Propagation constant of the plasma wave
β^*	Symmetry factor
Δf	Frequency bandwidth
$\Delta\phi_o$	Equilibrium potential
ϵ_m	Dielectric constant of the metal
ϵ_o	Permittivity of free space
ϵ_r	Permittivity of electrolyte
ρ	Resistivity of the electrolyte

1. INTRODUCTION

Microelectrode arrays or MEAs as they are commonly referred, were first described by Thomas *et al.* in 1972, for the purpose of obtaining extracellular recordings from the electrogenic cells cultured *in vitro*. Since then several advancements have been made, and with increasing demand, custom designed layouts have been developed as necessitated by the specific requirements. Nowadays MEAs play a significant role in the basic electro-physiological study of the cardiomyocytes (Reppel *et al.* 2004), and are employed in the conduction studies of the human embryonic stem cell derived cardiomyocytes (Kehat *et al.* 2002). In addition to the drug screening and the toxicological studies (Bal-Price *et al.* 2010; Ylä-Outinen *et al.* 2010), MEAs are also widely employed in measuring neuronal activity from acute tissue slices, primary cells and their cell lines (Gross 1979; Johnstone *et al.* 2010). The list continues, but nevertheless, depending on the application, the MEA is to be treated with suitable surface molecules prior to use, as cellular interaction with the MEA surface is mediated through these molecules.

The surface molecules are usually complex proteins or polymers with electrically charged groups, but as they are largely composed of carbon, hydrogen, and oxygen, they are inherently poor conductors of electricity. Their conductivity further varies with the orientation, molecular association, denaturation, and variations in the internal conformation. However, since these molecules have a decisive effect on the adhesion, migration, differentiation, and growth of the cells, it is essential to understand the impact of these coatings on the performance of the MEA, as large impedances can drastically affect the charge transfer capacity at the interface.

Studies employing electrical impedance spectroscopy have long been conducted to evaluate the influence of the coatings on the electrodes. Liu *et al.* (2010) experimented with a thin film of agarose coating on an array of interdigitated microelectrodes and noticed no significant difference in the magnitude of the impedance upon coating. However, the effect of collagen I on iridium oxide micro-needles was observed to be well pronounced by Karp *et al.* (2008), with the impedance increasing by more than 10 fold, except the coating was not intended for cell culture. Electrostatic self-assembly of alternating polyelectrolytes such as PEI or chitosan, with proteins laminin or gelatin was studied by He & Bellamkonda (2004), and these nano-scale multi layered coatings were not found to elicit any significant change in

the magnitude of the electrode impedance.

Although these studies provide quite conclusive results, the main objective of this thesis is to study the coatings used by the research groups at the Institute of Biomedical Technology (IBT), University of Tampere, Finland, and evaluate their influence on the overall impedance and the noise magnitudes of the MEA electrodes. The thesis also aims at determining the thickness and the surface texture of these surface molecules, using the stylus profilometer and the atomic force microscope (AFM) respectively.

Similar studies have been conducted by Bougas *et al.* (2011) utilising ellipsometry, wherein the change in the polarization of the incident radiation as it interacts with the material, quantified by the phase difference and the amplitude ratio is used with the McCrackin (1969) algorithm to determine the thickness of the protein coating. He & Bellamkonda (2004) employed quartz crystal microbalance to measure the thickness of the coating. Molecular adsorption on the electrode surface results in a decrease in the oscillation frequency of the quartz crystal, and the linear dependence between this frequency shift and the adsorbed mass provided by the Sauerbrey (1959) equation, is then used to determine the coating thickness.

However, compared to the two former techniques profilometer offers a relatively simple and a straight forward approach to measure the thickness of the coating. Besides, the other techniques mentioned above do not provide information pertaining to the uniformity of the coating.

The following chapter provides a brief explanation on the theory of microelectrode arrays, and the surface molecules utilised to coat the MEA surface. The electrochemical interface that develops along the electrode surface, and its influence on the overall impedance and the noise of the sensor is discussed as well, together with the working principle and the basics of the several measurement techniques employed in this study. The ensuing chapter focuses on the material and the methods employed in the experiments, including that involving the cells. The results are presented and discussed subsequently. The conclusions on the thickness and the effect of the coatings on the performance of the MEAs are made thereafter, along with the prospects for further deliberation in this regard.

2. THEORETICAL BACKGROUND

Electrogenic cells regulate vital processes in the human body such as neurotransmission, information processing, synchronised beating of cardiomyocytes etc., and the electrical activity of these cells can be studied through intracellular or extracellular methods. In intracellular technique, electrodes are inserted or clamped to the cell and the electric flux across the membrane is measured. External micro-transducers are employed in extracellular methods to measure ionic concentration outside the cell membrane. In either of these methods, the simultaneous and inter-dependant activity of the cells in response to environmental and/or contextual stimuli can be crucial, as in cellular signalling. In such cases, wherein the behaviour of the cells and/or the network characteristics are to be studied simultaneously at a high spatial resolution, microelectrode arrays are required. (Jones *et al.* 2011)

2.1 Microelectrode Array

Microelectrode array is a two dimensional grid of electrodes or micro-transducers, with at least one dimension small enough in the range of 0.1 to 50 μm (Montenegro *et al.* 1991). The electrodes are embedded in an insulating substrate, which is usually glass for *in vitro* applications, such that each electrode is independent of its neighbours, as presented in Figure 2.1. When coupled to a differential amplifier, these micro-transducers can measure voltage or current with respect to a common reference. (Jones *et al.* 2011)

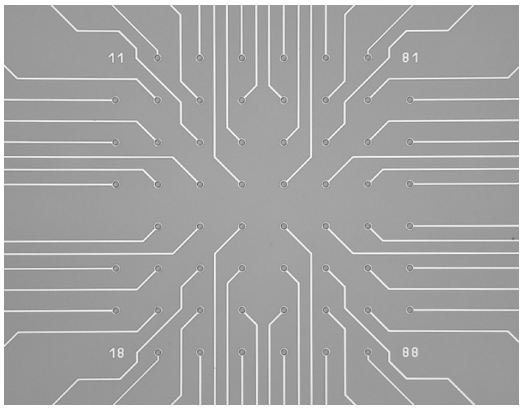

Figure 2.1: Circular, flat micro-electrodes aligned in a standard 8 × 8 grid, seen together with the tracks laid to establish contact with the external circuit. (Microelectrode Array Manual 2012)

In addition to measuring the potential or intrinsic activity of the cell, some MEAs are also capable of stimulating the electrogenic cells by delivering a current or voltage pulse, thereby eliciting a response which is recorded by the non-stimulating electrodes (Grumet *et al.* 2000; Wagennar *et al.* 2005; Hafizovic *et al.* 2007; Heer *et al.* 2007). Therefore in principle, MEA can be defined as a two dimensional array of voltage probes designed for electrical stimulation and/or monitoring of the electrical activity of the cell(s) (Fejtl *et al.* 2006). Based on the application or field of use, there are several types and/or layouts of MEAs available. Two of these commercial MEAs, the standard 60 electrode 8 × 8 MEA, and the 6 well MEA manufactured by Multi Channel Systems MCS GmbH, Reutlingen, Germany, are discussed below.

Standard 8 × 8 MEA

The standard 8 × 8 MEA has 60 electrodes arranged in a 8 × 8 layout as illustrated earlier. The electrodes in general are flat and circular, about 10 μm or 30 μm in diameter, and are positioned with an inter-electrode distance of 100 μm or 200 μm from the center of one another. However, depending on the requirement, one of these electrodes may be replaced with a large internal reference electrode as represented in the Figure 2.2(b).

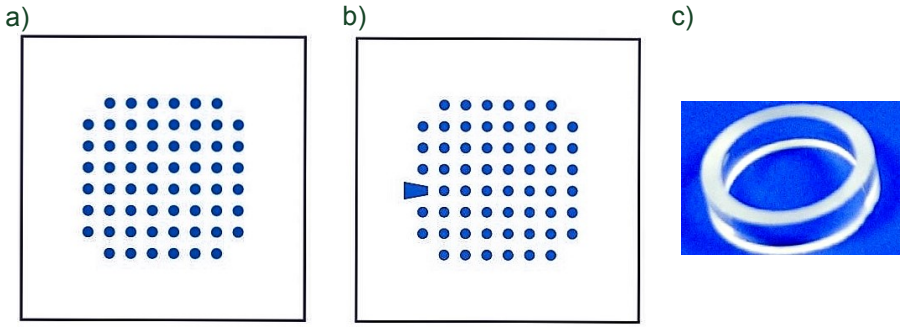

Figure 2.2: The electrode placement on the surface of the standard MEA without the reference electrode is illustrated in (a), and the same with the internal reference electrode is presented in (b). The glass ring that forms the culture chamber around the MEA electrodes is pictured in (c). (Multi Channel Systems MCS GmbH 2013)

Titanium nitride is used to make the electrodes, as it is very stable and suitable for long term experiments, lasting for several weeks or months. The standard tracks are either made of titanium or indium tin oxide, and the contact pads of titanium nitride. The MEAs are heat-stabilized, robust and reusable, hence they can be autoclaved and employed in a wide variety of procedures for *in vitro* cell, and tissue cultures. Glass rings similar to the one depicted in Figure 2.2(c) are then utilised to form the culture chambers. (Microelectrode Array Manual 2012).

6 Well MEA

The 60 electrode, 6 well MEA contains 6 distinct electrode chambers, with nine electrodes each, positioned in a 3 × 3 grid, together with an internal reference electrode in each chamber, as shown in the Figure 2.3. The electrodes are 30 μm in diameter, and are arranged with an inter-electrode distance of 200 μm.

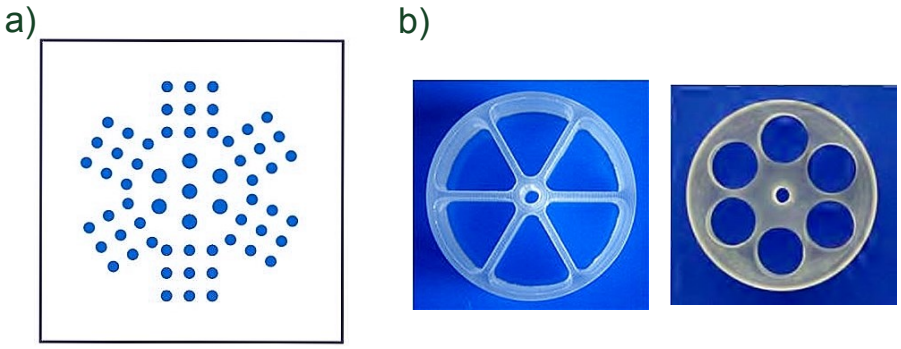

Figure 2.3: The electrode placement on the surface of the 6 well MEA is represented in (a). The rings used in isolating the MEA chambers are portrayed in (b). (Microelectrode Array Manual 2012)

At the center of the MEA is another reference electrode, used primarily for grounding purposes. All the reference electrodes are connected to each other. The electrodes and the contact pads are made of titanium nitride, whereas the tracks are made of titanium, with silicon nitride being employed as the insulator. The chambers are separated using glass or macrolon rings, so that six independent experiments can be carried out at once. The MEAs are heat-stabilized, robust and reusable, hence they can be autoclaved and utilised in a wide variety of procedures for *in vitro* cell, and tissue cultures. (Microelectrode Array Manual 2012)

2.2 MEA Coatings

Microelectrode arrays are preferred for cell cultures largely for the multi-site, non-invasive, simultaneous extracellular recordings that are obtained without mechanical stimulation of the cell; something that is hardly avoidable in conventional recording methods. The cells cultured on MEAs adhere firmly to the substrate and contract isometrically, thereby eluding from any motion artifacts that could affect the signal-to-noise ratio, usually abbreviated as SNR. However prior to culturing of cells and/or tissues, the substrate is pre-treated and coated with suitable surface molecules such as cellulose nitrate, fibronectin, collagen etc., as surface properties of the substrate have a decisive effect on adhesion, migration, differentiation, and growth of the cells. (Egert & Meyer 2005)

A few of these coating materials such as a) polyethyleneimine and laminin, b) gelatin, and c) Matrigel^{TM}, that are employed in neural and cardiac applications are examined in this section.

2.2.1 Polyethyleneimine and Laminin

Polymers are preferred attachment promoting factors, as they are inexpensive and easily synthesised, while some even exhibit biocompatibility and biodegradability (Lakard *et al.* 2004; Vancha *et al.* 2004). Polyethyleneimine or PEI as it is referred, is an organic polymer with a general backbone of $(CH_2CH_2NH)_n$, as represented in Figure 2.4. It can either be a linear or a branched polymer, and carries a cationic charge due to the high density of the protonated amino groups. The extent of protonation of the nitrogen atoms and by extension the overall charge density of PEI therefore depend upon the pH. On coating, these positively charged groups on the substrate bind with the negatively charged cell membrane, thereby preventing the cells from migrating. (He & Bellamkonda 2004; Product Information: Polyethyleneimine solution 2011)

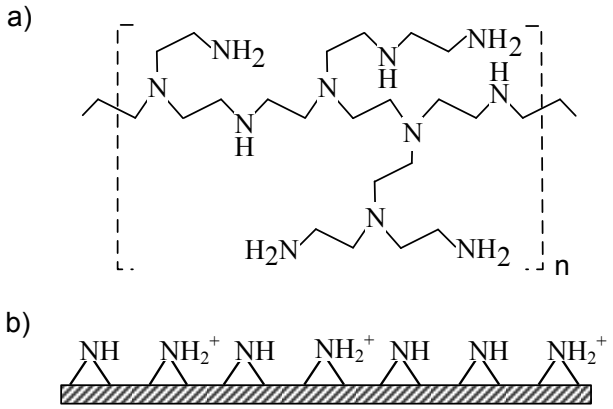

Figure 2.4: The repeating structural unit of PEI is represented in (a). The distribution of the chemical groups on the glass surface, after modification with PEI is illustrated in (b). (Liu et al. 2006; Product Information: Polyethyleneimine solution 2011)

Laminin, on the other hand, is an extracellular matrix glycoprotein and a cruciform heterotrimer composed of three different glycosylated polypeptide chains, α, β, and γ. Structurally they are large T-shaped molecules, comprising one long arm and two or three short arms, as depicted in the Figure 2.5. The long arm is in parts made of three chains, whereas the short arms are formed of just one chain each. (Aumailley *et al.* 2005)

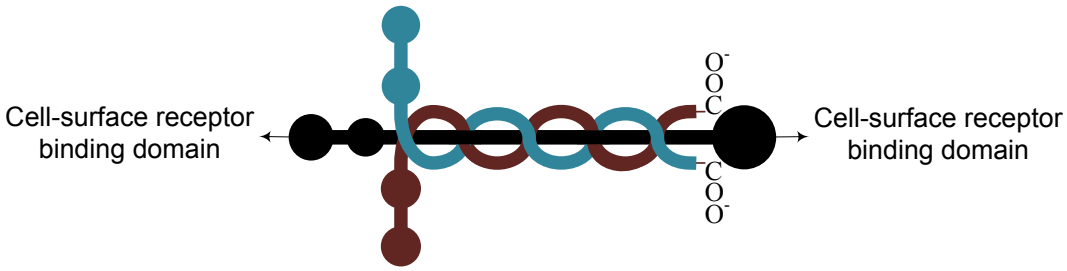

Figure 2.5: The structure of the laminin I molecule, a cruciform heterotrimer. (Liu et al. 2006)

Laminin is a very effective cell adhesive, and is quite extensively used for *in vitro* neuronal cultures, since it aids in cell (axon) development, differentiation and migration (He & Bellamkonda 2004). Besides, rapid adhesion of neurons to laminin permits even distribution of the cells, which otherwise tend to aggregate if the adhesion is slow (Lindsay *et al.* 1991).

The coating is prepared using electrostatic layer-by-layer assembly, as fine control over the layer thickness is achieved using this technique. The electrostatic force of attraction between the charged surface and the oppositely charged polycation is the basis for electrostatic layer-by-layer self assembly. In this case, the polycationic PEI first renders the negatively charged glass substrate positive (Egert & Meyer 2005) as illustrated in Figure 2.4(b). When laminin is added thereafter, the amino groups of PEI interact with the carboxyl groups of laminin, thereby forming the substrate for the cell culture. (He & Bellamkonda 2004; Liu *et al.* 2006)

2.2.2 Gelatin

Gelatin is a polypeptide that is obtained through thermal hydrolysis of collagen. It contains a heterogeneous mixture of high average molecular weight proteins that are extracted from the skin, bones, tendons, ligaments, etc. Based on the retrieval process followed, gelatin is classified as a) Type A when derived from acid-cured tissue, and b) Type B if obtained from lime-cured tissue. Gelatin contains carboxyl, amino, and guanidino groups on the side chains, which greatly influence on the charge it carries. However, Type A gelatin is electrically neutral in the physiological pH range. (Product Information: Gelatin 2013)

The exact structure of gelatin is difficult to determine, since the characteristics change when it is allowed to dry. At concentrations greater than 1 %, AFM images of gelatin reveal fibril like structures. However, gelatin in concentrations less than 1 % form spherical aggregates interspersed with the fibril like structures. (Yang & Wang 2009) It is employed in cultures, as cells, and in particular the endothelial cells adhere to gelatin quite well, and it does not interfere with the process of differentiation, unlike many other extracellular matrix proteins (Ingrid *et al.* 1998). Similar to

the coating procedure followed for PEI and laminin, gelatin is coated based on self assembly.

2.2.3 Matrigel™

Matrigel™, also known as Cultrex™ or just reconstituted basement membrane, is an extract of basement membrane proteins, from a tumour with abundant extracellular matrix proteins, the Engelbreth-Holm-Swarm mouse sarcoma. Laminin, followed by collagen IV, and heparan sulphate proteoglycans mainly constitute Matrigel™. (Kleinman & Martin 2005)

Matrigel™ remains as a liquid when maintained at a temperature of 4 °C, but when physiological conditions are mimicked, and the temperature is increased to 37 °C, the components polymerise to form a gel with ultra thin structures, that appear as interconnected sheets. This gel formation is highly dependent on temperature, with maximum polymerization taking place at 35 °C, and a lack of interaction at temperatures as high as 50 °C, suggesting thermal denaturation of a critical constituent. The gelled components, linked by relatively strong non-covalent bonds form a bioactive growth surface, that promotes attachment, and differentiation of several cell types, and hence is preferred in varied cell cultures. (Kleinman *et al.* 1985; Kleinman & Martin 2005)

Extensive dilution of Matrigel™ on the other hand, results in the formation of a thin protein layer at elevated temperatures. This is more suited for cell attachment, but not so much for differentiation studies. (Matrigel™: Guidelines for use 2012)

2.3 MEA Recordings

In order for MEA, or any other electrode for that matter, to be used in biomedical applications, a low impedance electrode-electrolyte interface is crucial. Especially when microelectrodes are involved in high resolution stimulation and/or *in vitro* monitoring of the electrogenic cells. A high impedance would cause large voltages to develop at the electrodes during stimulation, resulting in undesirable electrochemical reactions that can be harmful to the cells. In addition, the extracellular signals obtained from the neural cells, on the order of microvolts may be lost in the ionic fluctuations of the surrounding electrolyte. (Franks *et al.* 2005) The electrode-electrolyte interface, together with these factors affecting the MEA recordings such as impedance, and noise are elaborated below.

2.3.1 The Electrode-Electrolyte Interface

When the MEA electrodes are immersed in an electrolyte, they are electrically neutral at the very instant of contact with the solution. However, anisotropic forces

instantaneously act on the particles along the phase boundary, resulting in the accumulation or redistribution of charges at the metal-electrolyte interface. Furthermore, transfer of electrons between the electrode and the electrolyte results in the formation of an electric field across the interface. This in turn accelerates oxidation or loss of electrons ($A \rightarrow A^+ + e^-$), and inhibits reduction or the gain of electrons ($A^+ + e^- \rightarrow A$), until an equilibrium is reached eventually, whereby the currents induced due to the transfer of electrons to and from the electrode are balanced. (Borkholder 1998; Bockris *et al.* 2002)

The excess charge on the electrode also impacts the electrolyte by orienting the water dipoles along the surface of the electrode, thereby forming a hydration sheath as illustrated in Figure 2.6. Furthermore, partly oblivious to the electrode charge, chemically dependent adsorption or specific adsorption of ions occur along the electrode surface, further affecting the space charge density at the interface. These ions are interspersed with the oriented dipoles as can be observed from Figure 2.6. (Borkholder 1998; Bockris *et al.* 2002)

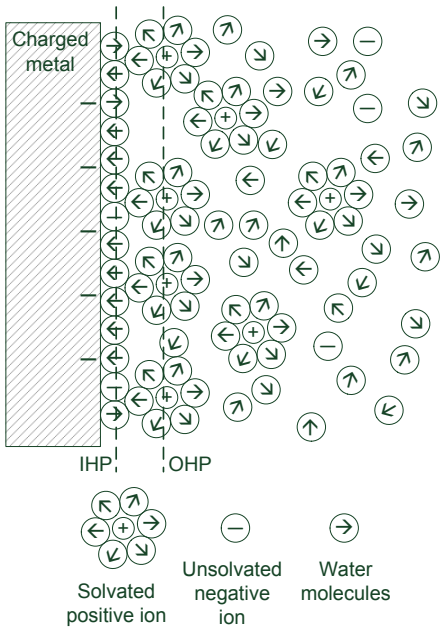

Figure 2.6: The schematic representation of the electrified electrode-electrolyte interface, adapted from Bockris et al. (2002).

The locus of centres of these ions, or the oriented dipoles as described in some texts is known as the inner Helmholtz plane, IHP. Closely following the water dipoles are the sheath of solvated ions, whose locus of centres is referred to as the outer Helmholtz plane, abbreviated here as OHP. The net outcome of the arrangement of these charges, and the oriented solvent dipoles is the electric double layer, an electrified interface that describes the inter-phase region across the electrode-electrolyte

phase boundary. Several theories have been developed in order to define this interface, as will be discussed below. (Borkholder 1998; Bockris *et al.* 2002)

2.3.2 The Electrode-Electrolyte Interface Impedance

Electrode-electrolyte equivalent circuit models using passive elements have been proposed by many, in order to understand and study the physical process occurring at the interface. Based on one such circuit model put forth by Randles (1947), the physical quantities primarily contributing to the interface impedance are a) constant phase angle impedance or the impedance due to interface capacitance, Z_{CPA}, b) charge transfer resistance, R_{ct}, c) solution resistance, R_s, and d) Warburg impedance, Z_w, as modelled in the Figure 2.7 (cited in Niklasson *et al.* 2005).

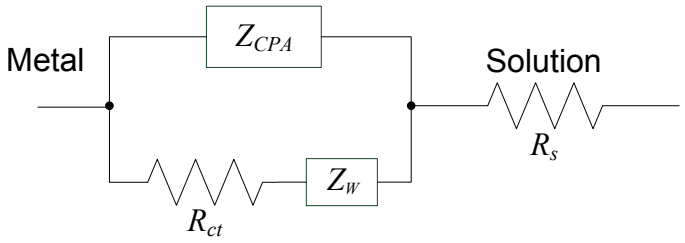

Figure 2.7: Equivalent circuit of the electrode-electrolyte interface. Modified from Randles (1947), cited in Niklasson et al. (2005).

Impedance due to Interface Capacitance

Interface capacitance is the double layer capacitance at the interface of the metal electrode and the electrolyte. Initial theories formulated by Helmholtz and Perrin suggest the electrified field at the interface to constitute two rigid sheets of charge densities, resembling a parallel plate capacitor, both equal in magnitude but opposite in sign. The Helmholtz interface capacitance, C_H is then presented using the empirical relation,

$$C_H = \frac{\epsilon_o \epsilon_r}{d_{OHP}} \tag{2.1}$$

where, d_{OHP} represents the thickness of the double layer, ϵ_o is the permittivity of free space, and ϵ_r is the permittivity of the electrolyte. However, this simple model is inadequate, as it fails to account for the dependence of capacity over potential. Gouy and Chapman modified the model by liberating the ions and rendering them mobile. This exposes the ions to thermal forces, in addition to the electric forces experienced from the electrode. The charge density originally concentrated at the OHP, diffuses with the increasing distance away from the electrode, until it reaches zero, wherein motion due to the thermal forces reign supreme. (Bockris *et al.* 2002)

The Gouy-Chapman capacitance, C_G in this case is obtained as,

$$C_G = \frac{\epsilon_o \epsilon_r}{L_D} \cdot \cosh \frac{Z\phi_o}{2U_t} \tag{2.2}$$

Here, Z is the ionic charge of the solution, U_t is the thermal voltage, and L_D is the Debye length, provided by the equation,

$$L_D = \frac{\epsilon_o \epsilon_r U_t}{2n^o Z^2 \mathrm{q}} \tag{2.3}$$

The variable n^o denotes the bulk number concentration of the ions in the solution, and q represents the elementary charge. The model is still considered a failure, as it overestimates the capacitance, partly because of neglecting the ion-ion interactions, and the change in the dielectric constant. Stern combined the concept of bound ions at the interface with the diffused ion cloud beyond, and synthesised the interface capacitance, C_I as in equation 2.4; A combination of Helmholz capacitance, and Gouy-Chapman capacitance in series. (Bockris *et al.* 2002)

$$\frac{1}{C_I} = \frac{1}{C_H} + \frac{1}{C_G} = \frac{d_{OHP}}{\epsilon_o \epsilon_r} + \frac{L_D}{\epsilon_o \epsilon_r \cosh \frac{Z\phi_o}{2U_t}} \tag{2.4}$$

The effect of specific adsorption of ions along the surface of the electrode, on the interface capacitance is not studied here, owing to complexity. The constant phase angle impedance is the measure of the non-faradaic impedance, and is expressed as,

$$Z_{CPA} = \frac{1}{(j\omega Q)^n} \tag{2.5}$$

The variable Q denotes the magnitude of C_I, n is an empirical factor representing the surface inhomogeneities, such that $0 \leq n \leq 1$, and $\omega = 2\pi f$. When $n = 1$, Z_{CPA} is purely capacitive, corresponding to the interface capacitance. (Franks *et al.* 2005)

Charge Transfer Resistance

Charge transfer resistance is a characteristic quantity, indicating the inherent speed of the faradaic charge transfer occurring at the electrode-electrolyte interface by means of oxidation-reduction reactions. It is given by the expression,

$$R_{ct} = \frac{RT}{FzJ_o} \tag{2.6}$$

Here, R is the gas constant, T is the temperature, F is the Faraday's constant, z is the number of electrons involved in the redox reaction, and J_o is the equilibrium exchange current density, whose magnitude can be acquired from the following

equation,

$$J_o = Fk_c c_A e^{-\frac{\beta^* F \Delta\phi_o}{RT}} \tag{2.7}$$

where, k_c is the rate constant of the reduction reaction, c_A is the concentration of the ions A in the solution at the interface, β^* is the symmetry factor, and $\Delta\phi_o$ is the equilibrium potential. (Franks *et al.* 2005)

Solution Resistance

Solution resistance is the resistance measured between the working and the reference electrodes. In other words, it is the resistance encountered by the current when spreading from the electrode out into the solution. On the assumption that the working electrode is rounded and surrounded by an electrolyte, and that the counter electrode is infinitely large, R_s is obtained using the formula,

$$R_s = \frac{\rho}{4r} \tag{2.8}$$

The parameter r represents the radius of the electrode, and ρ denotes the resistivity of the electrolyte. Unlike C_I, and R_{ct}, solution resistance depends upon the geometric area and not the total surface area of the electrode. (Franks *et al.* 2005)

Warburg Impedance

When an alternating current field is applied, the negative ions diffuse towards the electrode during the positive phase of the field, repelling the positive ions away, until the negative phase begins and the reverse occurs. This diffusive motion of the ions under the influence of the alternating current field contributes to the Warburg impedance. It has been shown that the impedance has a phase angle of 45 degrees, and is proportional in magnitude to $\omega^{-\frac{1}{2}}$. The impedance value is given as,

$$|Z_w| = \frac{1}{2}\frac{RT}{z_i F}^2 \cdot \frac{1}{c_i}\sqrt{\frac{1}{D_i}} \tag{2.9}$$

Here, z_i is the charge of the ion concerned, c_i is its concentration, and D_i is its diffusion coefficient. However, at higher frequencies and concentration, Warburg impedance is almost negligible when compared with the other impedance values. (Warburg 1899, cited in Bockris *et al.* 2002)

2.3.3 Electrode-Cell Interface Impedance

The electrode-cell interface can be represented electrically as shown in Figure 2.8. It includes the electrode-electrolyte interface which features the interface capac-

itance, charge transfer resistance, and the diffusion related Warburg impedance. The spreading resistance R_s can be neglected in this case, as the electrode radius is larger, at least twice or thrice in magnitude than the average distance between the cell and the electrode (Joye *et al.* 2009).

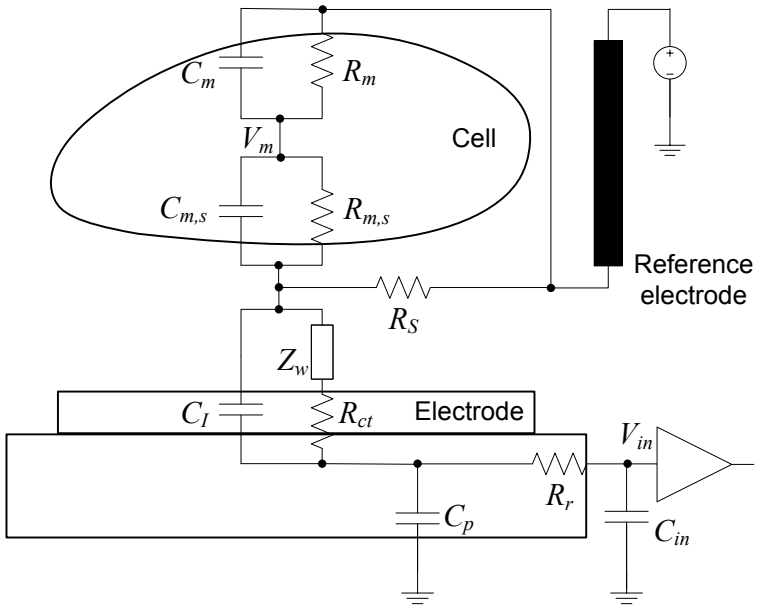

Figure 2.8: Electrical equivalent circuit model of the cell-electrode interface as represented by Guo et al. (2012).

The three component equivalent circuit of the electrode-electrolyte interface can be equivalently represented by a frequency dependant resistor $R_{es}(\omega)$, and capacitor $C_{es}(\omega)$ placed in parallel, such that,

$$R_{es}(\omega) = R_{ct} + R_w(\omega) + \frac{I_w(\omega)^2}{R_{ct} + R_w(\omega)} \tag{2.10}$$

$$C_{es}(\omega) = C_I - \frac{1}{\omega} \frac{I_w(\omega)}{(R_{ct} + R_w(\omega))^2 + I_w(\omega)^2} \tag{2.11}$$

The cell forms a seal with the electrode at the electrode-cell interface, which although distributed can be represented electrically through a seal resistance R_S. The cell membrane also exhibits capacitance C_m, and resistance R_m parallel to the seal resistance. The collective membrane capacitance and resistance within the seal area are represented as $C_{m,s}$ and $R_{m,s}$ respectively, whereas the equivalent electrode capacitance within the seal area is represented as $C_{es,s}$. The resistance of the routing path R_r, which usually employs metal wires is less than 1 Ω, and thus negligible. Besides the input capacitance C_{in}, parasitic capacitance C_p develops at the interface,

which can be attributed to two factors,

1. The coupling capacitance between the routing metal of the electrode and the ground plane, which could be a conductive substrate, solution, or the routing metal of another electrode.

2. The double layer or interface capacitance at the region of the electrode not covered by the cell. (Guo *et al.* 2012)

2.3.4 Noise

Noise is intrinsic in all measurement systems and signal sources. In the measurements using MEAs though, the noise could be broadly confined into a) electrode noise, b) biological noise, c) electronic noise, and d) noise from external factors. Noise due to the external electromagnetic sources, such as power line interference at 50 Hz, and electronics can be reduced through careful shielding of the measurement setup, and via design of low noise electronic configurations respectively. The two other noise sources electrode noise, and biological noise are discussed in detail below. (Borkholder 1998)

Electrode Noise

Electrode noise is the intrinsic noise generated at the electrode-electrolyte interface. It has been empirically determined to be thermal by Gesteland *et al.* (1959), and the RMS noise voltage in a narrow frequency bandwidth is given by the standard Johnson noise equation as,

$$V_{rms} = \sqrt{4kTR_{es}\Delta f} \tag{2.12}$$

where, k is the Boltzmann's constant, T is the absolute temperature, and Δf is the noise bandwidth. It is to be noted that R_{es} is the effective resistance of the electrode at the same frequency. As in practice, the impedances vary with frequency due to diffusion related processes. Also, the equation assumes that the system is at thermal equilibrium, indicating that the current flowing through the electrode is zero, and that no chemical reaction is taking place at the surface of the electrode. (Gesteland *et al.* 1959)

At the cell-electrode interface though, the electrode noise is influenced by both R_S, and R_{es}. The frequency dependant noise models developed by Guo *et al.* (2012) at the electrode-electrolyte and cell-electrode interface are presented in Figure 2.9, and Figure 2.10 respectively.

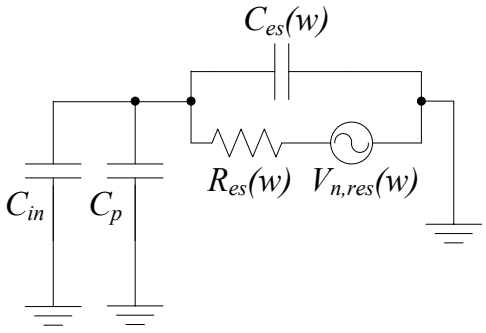

Figure 2.9: The frequency dependant noise model at the electrode-electrolyte interface, adapted from Guo et al. (2012).

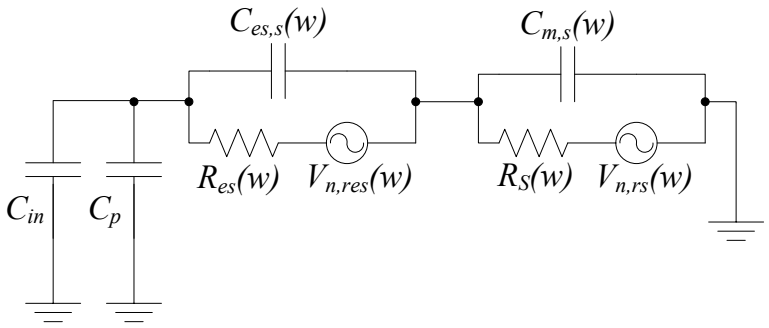

Figure 2.10: The frequency dependant noise model at the cell-electrode interface (Guo et al. 2012).

Equivalent noise circuits have been derived by Guo *et al.* (2012) based on the noise models in Figure 2.11. Here i_{sig} is the ionic current from the cell, and $i_{n,rs}$, and $i_{n,res}$ are the noise currents at R_S and R_{es} respectively. Using these equivalent circuits, the amplitude of R_{es} noise low pass filtered to the amplifier input is determined as,

$$V_{n,in,res} = i_{n,res} R_{es} \frac{1 + sR_S C_{m,s}}{[1 + sR_{es}(C_{es,s} + C_{in} + C_p)][1 + sR_S(C_{m,s} + C_{in} + C_p)]} \quad (2.13)$$

The magnitude of the R_S noise, low pass filtered to the amplifier as obtained by Guo *et al.* (2012) is,

$$V_{n,in,rs} = i_{n,rs} R_S \frac{1 + sR_{es} C_{es,s}}{[1 + sR_{es}(C_{es,s} + C_{in} + C_p)][1 + sR_S(C_{m,s} + C_{in} + C_p)]} \quad (2.14)$$

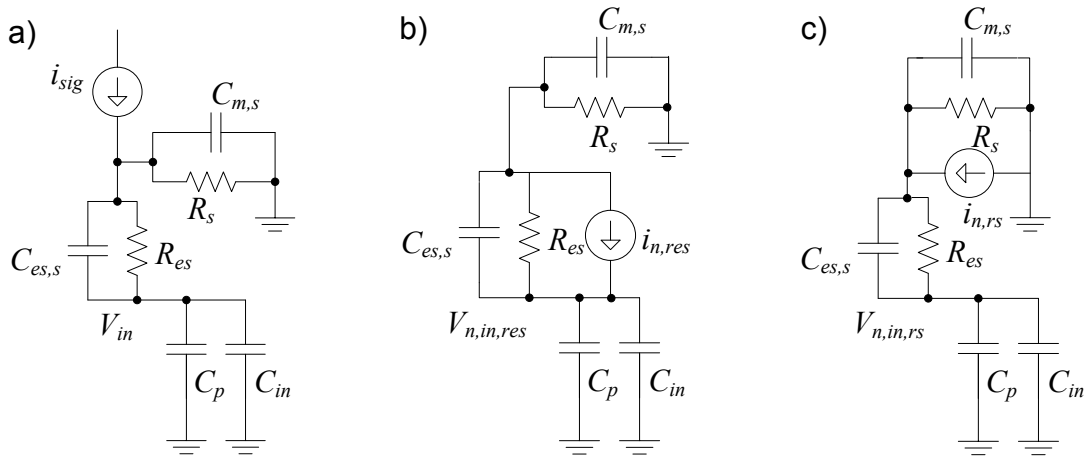

Figure 2.11: The equivalent circuits utilised by Guo et al. (2012) in determining the noise across the resistances R_S, and R_{es}.

Biological Noise

Biological noise is inherent to the living system and is often in the same spectral band as the signal of interest, as in the case of action potential measurement, where electrical activity from the neighbouring cells could contribute to the overall noise. However in the study of impedance characteristics of the cell membrane, biological noise is much harder to determine with the changes in cell-substrate coupling, and motility of the cell. (Borkholder 1998)

Experiments conducted by Borkholder (1998) indicate a possible change in impedance with regard to cellular motility, and swelling of the cells. Biological noise from the neighbouring cells can be subdued to an extent by inhibiting cellular attachment in the regions at close proximity with the electrode. In addition, isolation from any uncorrelated noise is also possible using suitable signal processing techniques such as averaging. However, there are no electronic or averaging techniques to do away with the consequence of motility, and/or swelling of the cell on the overall noise. (Borkholder 1998)

2.4 Measurement Techniques

In order to obtain the impedance and noise characteristics of the MEA, together with the surface characterization of the coated surfaces, several different measurement methods need to be adopted. The working principle and other related information relevant to the measurement techniques implemented in this work such as a) impedance analysis, b) surface texture analysis, and c) surface plasmon resonance are briefly discussed in this section.

2.4.1 Impedance Analysis

Two distinguished techniques can be employed in the analysis of impedance, a) I-V method and b) AC impedance bridge compensation method.

The I-V method involves direct phase sensitive recording of the sample current and voltage, wherein an electrical signal comprising of a known voltage or current is applied, and the corresponding response current or voltage is recorded. The approach differs based on the type of stimulus used such as a) step function of voltage, b) signal composed of white noise, and c) single frequency voltage or noise signal. The three classifications are further discussed below.

Step function of voltage

A step function of voltage *V(t)*, such that $V(t) = V_0$, for $t > 0$; and $V(t) = 0$, for $t < 0$ is applied to the system at time, $t = 0$, and the time varying current, *i(t)* is measured. The impedance obtained as a ratio of V_0 and *i(t)* is referred to as the indicial impedance. Fourier transform is applied thereafter to the time varying results, to obtain the relevant frequency dependent impedance. Suitable windowing techniques are necessary to correct the distortions arising due to the non-periodicity of excitation. Besides being experimentally easy to accomplish, the advantage of this method is that the rate of electrochemical reaction occurring at the interface can be controlled with the applied voltage, V_0. The disadvantages on the other hand include the need to perform transformations, and since the signal-to-noise ratio varies between different frequencies, the impedance is not well determined over the frequency range of interest. (Macdonald & Johnson 2005)

Signal composed of white noise

A signal *V(t)*, composed of random white noise is applied to the interface, and the resulting current is measured. Fourier transform is then employed to obtain the frequency dependent impedance. Since the signal is applied to the interface only for a short period of time, rapid data collection is possible using this approach. Also, a sum of sine waves could be used instead of white noise for excitation, as it offers better signal to noise ratio at each desired frequency. The limitations of this technique however include the need for white noise and Fourier transformations. (Macdonald & Johnson 2005)

Single frequency voltage or current signal

Voltage or a current signal with a single frequency is applied to the interface, and the resulting current, or phase and amplitude, or real and imaginary parts of impedance are measured either using analog circuits or through fast Fourier transform of the response. Several commercial equipment exploit this approach owing to its ability to achieve a relatively better signal-to-noise ratio in the desired frequency range. (Macdonald & Johnson 2005)

The second method in impedance analysis is the AC impedance bridge compensation technique. It requires balancing of the current flowing through the sample impedance Z_s^* and the compensation impedance Z_c^*, as illustrated in Figure 2.12. (Kremer & Schönhals 2003)

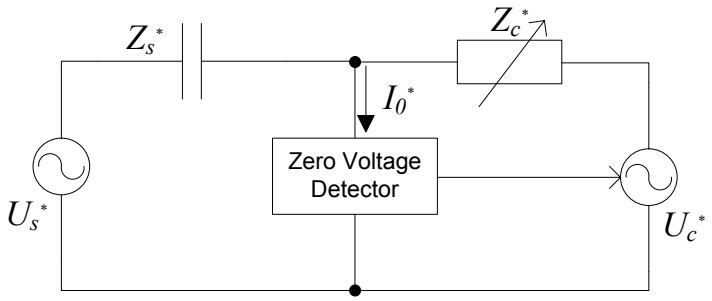

Figure 2.12: The schematic of an AC impedance bridge as designed by Kremer & Schönhals (2003).

As the known voltage U_s^* forces a current through the sample impedance, the variable amplitude-phase generator drives a current through the compensation impedance. The difference in currents between the two hands of the bridge is detected by the zero voltage detector, which then suitably alters the amplitude and the phase of the of amplitude-phase generator, so that the bridge is balanced and the net current I_0^* is zero. The system is then said to be in equilibrium, and the impedance is given as,

$$Z_s^*(\omega) = \frac{U_s^*(\omega)}{U_c^*(\omega)} \cdot Z_c^*(\omega) \tag{2.15}$$

AC impedance bridges operate typically over a frequency range of 10 Hz to 10 MHz, at relatively short measurement intervals, and can measure impedances upto 100 MΩ. (Kremer & Schönhals 2003)

2.4.2 Surface Texture Analysis

Surface texture refers to any local deviation from the nominal or ideal surface that forms the surface topography, and includes surface roughness, waviness, lay, and flaws. Surface roughness in general represents the differential height of the surface in relation to the reference plane, obtained along an individual line profile, or along a batch of parallel line profiles rendering surface maps. Surface roughness is mostly characterised by one of the two following statistical height descriptors,

R_a is the arithmetic average deviation from the mean, and is evaluated using the formula,

$$R_a = \frac{1}{L}\int_0^L |z - m| \mathrm{d}x \tag{2.16}$$

$$m = \frac{1}{L}\int_0^L z \mathrm{d}x \tag{2.17}$$

where, L is the profile length, $z(x)$ is the profile height measured from the reference line. (Bhushan 2013)

R_q is the RMS value of surface roughness, obtained by the equation,

$$R_q = \sqrt{\frac{1}{L}\int_0^L z^2(x) \mathrm{d}x} \tag{2.18}$$

Other height descriptors in limited use are R_p, R_v representing the maximum peak height from the mean, and the maximum valley depth from the mean respectively, and R_z, R_{pm} portraying the average peak-to-valley height, and average peak-to-mean height correspondingly. (Bhushan 2013)

Surface roughness can be acquired with an AFM using three different approaches, a) contact method, b) intermittent contact method, and c) non-contact method as described below.

Contact Method

Contact method requires the measurement component to establish physical contact with the measurement surface or sample. The methodology in this case is explained with respect to a stylus profilometer. The stylus arm is positioned against the sample and traversed across the stationary sample at a constant speed as illustrated in Figure 2.13. Relative movement of the sample surface with reference to the stylus is also plausible. The vertical displacement of the stylus, corresponding to the surface variations are mechanically coupled to a transducer such as a linear variable differential transformer, LVDT. The LVDT generates a corresponding analog signal,

that is amplified, conditioned, digitised, and rendered as a function of the position of the stylus tip. (Chi *et al.* 2010; Bhushan 2013)

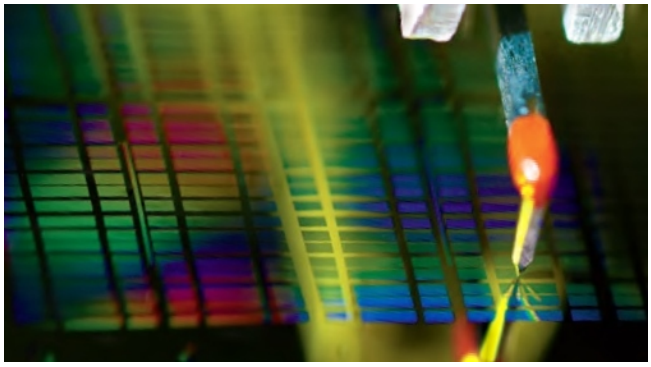

Figure 2.13: The image of the mechanical stylus positioned in contact with the sample surface, obtained from Dektak XT Stylus Profiling System - Brochure (2011).

Although the method is demonstrated to detect minute surface variations, the local pressure developed along the area of the substrate in contact with the stylus may effect localised, yet significant elastic deformation of the measured sample. When the pressure exceeds the hardness of the material, plastic deformation can occur, resulting in measurement errors and undesirable damage to the sample. Besides, the finite dimensions of the stylus tip may distort the surface profile, exaggerating the radius of curvature of the peaks and/or misrepresenting the valleys as cusps, as shown in Figure 2.14. (Bhushan 2013)

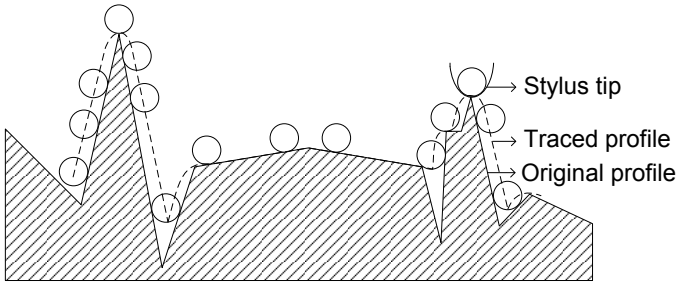

Figure 2.14: The misrepresentation of the profile owing to the finite size of the stylus tip, as presented by Bhushan (2013).

Intermittent Contact Method

Intermittent contact method, as the name suggests involves slight tapping of the surface by the oscillating cantilever assembly. The cantilever is vibrated at a certain amplitude, referred to as the free amplitude, before it engages the sample. The amplitude is maintained large enough, so as to prevent the tip from sticking to the sample under the influence of the adhesive forces. (Bhushan 2008)

The influence on the amplitude as it contacts the surface is used to determine the set point, which is the ratio of the vibration amplitude after engagement with the sample to the amplitude before engagement in free air. A reduced amplitude means a lower set point, which in turn reflects the closer mean tip-to-sample distance. The schematic representation of intermittent contact mode is provided in Figure 2.15. Intermittent contact method can be used for measuring the topography of soft substrates, as it employs a lower average load compared to the contact mode, thereby minimizing the effect of friction and other lateral forces, and reducing sample damage. (Bhushan 2008)

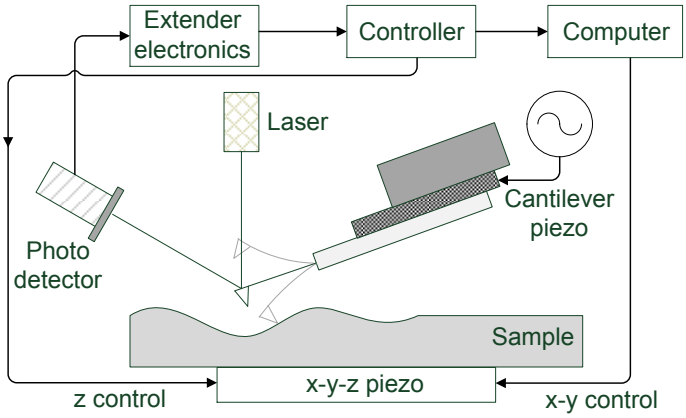

Figure 2.15: Schematic representation of the intermittent contact mode used in topography measurements, adapted from Schirmeisen et al. (2008).

Non-Contact Method

Non-contact method is principally based on the static electric repulsive forces between the ion cores, and the attractive forces that exist between the valence electrons and the ion cores, of atoms placed a short distance apart. Unlike the intermittent contact approach, it employs cantilevers that are made to vibrate near the sample surface, from as close as a few tens to hundreds of nanometres. This precise tip-sample spacing control enables the cantilever to steer clear of any physical contact with the surface, as presented in Figure 2.16. (True Non-Contact Mode^{TM} 2013)

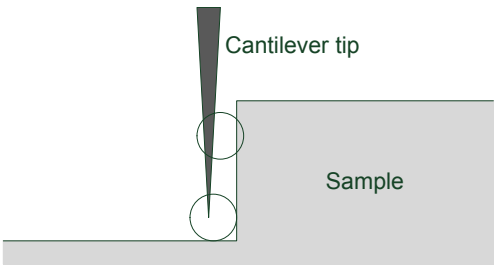

Figure 2.16: The interaction between the cantilever tip and the sample in non-contact method (True Non-Contact Mode^{TM} 2013).

As the distance between the tip of the probe and the atoms on the sample becomes much shorter, repulsive Coulomb interactions between the ion cores are recorded. Whereas when the distance gets relatively large, the ion cores are transformed into electric dipoles, owing to the valence electrons in the neighbouring atoms. This generates a van der Waals force of attraction between the electric dipoles. Due to this attractive force between the tip of the probe and the atoms on the sample surface, the cantilever vibration near its resonant frequency experiences a shift in the spring constant, given by the following expression as,

$$k_{eff} = k_o - \frac{\delta F^*}{\delta z} \tag{2.19}$$

where, k_o is the intrinsic spring constant, and $F' = \delta F^*/\delta z$ is the force gradient. As the attractive forces are applied, k_{eff} becomes smaller than k_o, which renders the force gradient positive, and the interaction between the surface and the tip stronger. (True Non-Contact Mode^{TM} 2013)

Non-contact mode therefore aids in preserving the sensor tip and the sample. It however risks accidental contact of the tip with the sample, in which case the meniscus force of the liquid atop the sample may render it inoperable (Non-Contact Mode AFM vs. Tapping Mode AFM 2013).

2.4.3 Surface Plasmon Resonance

Surface plasmon resonance, abbreviated as SPR is the charge-density oscillation that occurs at the interface of two media having dielectric constants of opposite signs, such as a metal and a dielectric. The surface plasma wave is a transverse magnetic electromagnetic wave, wherein the magnetic vector is parallel to the plane and perpendicular to the direction of the propagation of the surface plasma wave. The propagation constant of the plasma wave at the interface between the semi-infinite dielectric and the metal is given by the formula,

$$\beta = k_n \sqrt{\frac{\varepsilon_m n_s^2}{\varepsilon_m + n_s^2}} \tag{2.20}$$

Here, k_n represents the free space wave number, ε_m is the dielectric constant of the metal, and n_s denotes the refractive index of the dielectric. Although any substrate satisfying the relation $\varepsilon_{mr} < -n_s^2$, where ε_{mr} is the real part of the dielectric constant of the metal, may be supported, silver and gold are commonly preferred at optical wavelengths. In the visible and the near infrared spectrum, the plasma wave propagates with high attenuation owing to high losses in the metal. Also, the electromagnetic field is highly asymmetric, and exhibits higher localization in the

dielectric. (Homola *et al.* 1999)

SPR Sensors and Sensing Configurations

An SPR optical sensor chiefly constitutes a) an optical system, b) a transducing medium that relates the optical and chemical domains, and c) the electronics to support the optics and permit data processing. The optical system in turn comprises the radiation source and an optical structure that excites the plasma wave. Thin layers of surface plasmon active metals such as gold and silver are often manufactured by vacuum evaporation and sputtering for this purpose. While silver exhibits increased sensitivity, long term stability is poor. The transducing medium which varies depending on the application "transforms any changes in the quantity of interest to changes in the refractive index, which can be determined by optically interrogating the surface plasma wave". During the interrogation of the surface plasma wave, the electronic system generates and processes the electronic signal. Stability, sensitivity, and resolution are determined by the nature of the optical system and the transducing medium, whereas selectivity and response time are primarily dependent upon the transducing medium. (Homola *et al.* 1999)

Excitation of the surface plasma wave cannot be achieved through direct incidence of the optical wave at the metal-dielectric interface, since the propagation constant of the plasma wave is invariably high when compared to the propagation of the optical wave in the dielectric. This requires a change in momentum of the incident wave, which is accomplished through attenuated total reflection in prism couplers and optical wave-guides, and/or through diffraction from the surface of the gratings, as discussed below. (Homola *et al.* 1999)

Optical Prism Coupler based SPR Sensor

SPR sensors based on prism couplers use two different methods to bring about plasma excitation using light, a) Kretschmann configuration, and b) Otto configuration. Optical prism couplers based on Kretschmann's approach are most widely employed in SPR sensors. According to this configuration, the light incident on the interface between the prism coupler and the thin metal layer is totally reflected at the interface, as illustrated in Figure 2.17. In this process though, the incident light excites the plasma wave at the outer boundary of the metal layer by tunnelling through evanescently. (Homola *et al.* 1999)

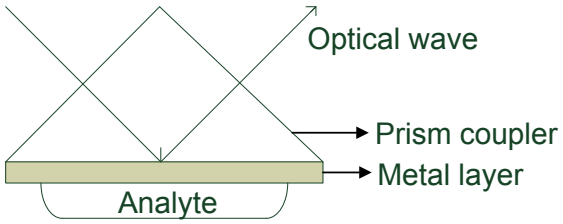

Figure 2.17: The prism coupler based SPR system as presented by Homola et al. (1999).

Grating Coupler based SPR Sensor

Grating couplers diffract the incident beam into a series of beams, directed at varied angles away from the periodically distorted metal-dielectric interface, as presented in Figure 2.18. The momentum of these waves is multiples of the grating wave vector and the components of momentum of the incident beam. (Homola *et al.* 1999)

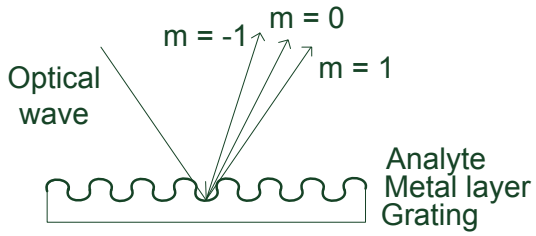

Figure 2.18: The SPR configuration based on the grating coupler system (Homola et al. 1999).

Although precise control over the thin metal layer is not necessary, the mathematics involved in modelling of the grating and/or its response is more complex than the prism based systems, and hence data analysis is difficult. One other drawback of grating based couplers is that, the incident beam traverses through the sample before diffraction, and therefore requires the analyte, and the flow cell to be optically transparent. (Homola *et al.* 1999)

Optical Waveguide based SPR Sensor

Waveguide based SPR sensors, as presented in Figure 2.19 are in principle similar to the Kretschmann's configuration of optical prism couplers. The light guided by the waveguide evanescently penetrates the metal layer, and when the guided mode phase-matches the surface plasma wave, a plasma wave is excited at the outer surface of the metal. (Homola *et al.* 1999)

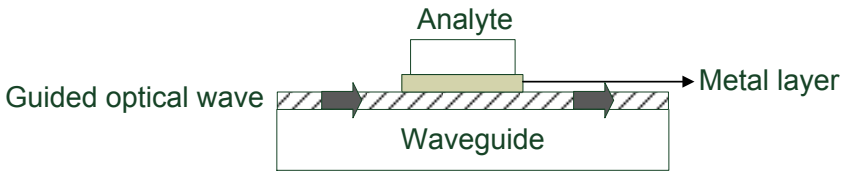

Figure 2.19: The optical waveguide based SPR system as represented by Homola et al. (1999).

Despite the design constraint, it implements all the main SPR detection techniques corresponding to the bulk prism based sensing devices. In addition to its ruggedness, and small size, this approach also provides numerous other enticing features, such as efficient control of light properties, stray light suppression, etc. (Homola *et al.* 1999)

3. RESEARCH METHODS AND MATERIALS

The effect of the surface coatings on the impedance and noise characteristics of the MEA is evaluated through a series of experiments. MEAs with two different layouts are studied, and the surface texture of the coated materials such as the surface roughness, and the coating thickness are analysed. In addition, an attempt is made by mimicking the cell culture environment, to realise the repercussions on the real life applications. The materials and methods employed in the series of measurements performed as part of this work are discussed in detail below.

3.1 MEA Setup

Commercial six well MEAs, manufactured by Multi Channel Systems MCS GmbH, Reutlingen, Germany, are used for the measurements alongside the standard 8×8 MEAs, as presented in Figure 3.1.

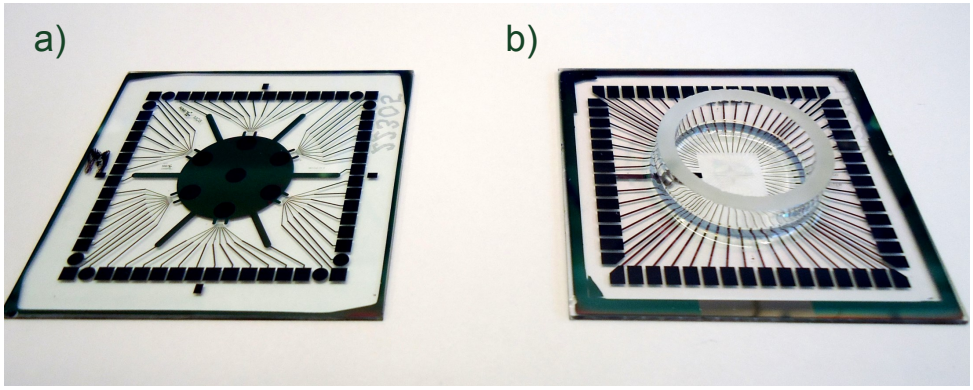

Figure 3.1: The 60 electrode 6 well MEA is imaged in (a), and the standard 8×8 MEA with an internal reference electrode and the glass ring is presented in (b).

The six well MEA contains 60 electrodes altogether, with each well comprising nine electrodes arranged in a 3×3 grid, together with a reference electrode. The standard 8×8 MEA also comprises 60 electrodes, including a large internal reference electrode, but the electrodes are positioned in a 8×8 grid. In both these MEAs, the electrodes are 30 μm in diameter, and are spaced at a distance of 200 μm from the center of one another. The electrodes and the contact pads are coated with titanium nitride, whereas the tracks are made of titanium, with silicon nitride being used as the insulator. (Microelectrode Array Manual 2012)

3.1.1 Polydimethylsiloxane (PDMS) Structures

Polydimethylsiloxane or PDMS structures are used as culture chambers to limit and hold the coating reagents, the cells to be seeded, and the buffer or the culture medium over the MEA. The structure establishes a reversible bond with the MEA substrate owing to van der Waals interaction, resulting in a water tight seal (McDonald *et al.* 2000). The bond strength is strong enough to hold on even during long term cultures, however it can be detached any time through peeling.

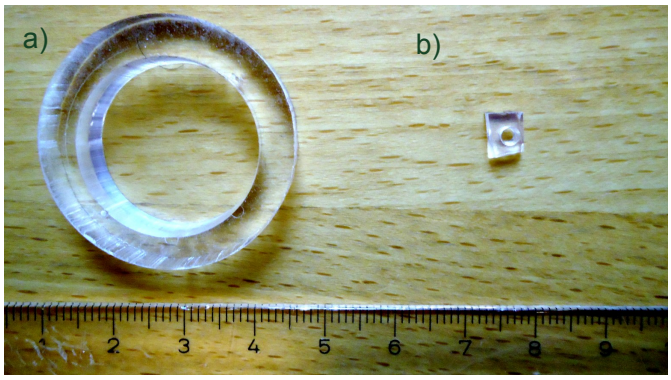

Figure 3.2: The open PDMS ring used with the 6 well MEA is imaged in (a), and the micro-well PDMS structure surrounding the electrode area of the standard MEA is pictured in (b).

In this experiment, PDMS rings of diameter 22 mm are custom made to form the well in case of the 6 well MEAs, whereas micro well structures about 2 mm in diameter are used to isolate the electrode area in the standard MEA, as shown in Figure 3.2. PDMS is preferred over other materials as it is a biocompatible polymer (Kreutzer *et al.* 2009), with mechanical properties similar to that of the human soft tissue (Wang *et al.* 2010). It is impervious to most chemicals (Mata *et al.* 2005), permeable to gas (Merkel *et al.* 2000), and is optically transparent down to the wavelengths of 290 nm (Shih *et al.* 2006). Moreover, it offers good thermal and electrical stability (Hemmilä *et al.* 2012), and is capable of replicating structures as small as a few nanometres (Xia & Whitesides 1998).

However PDMS has a few shortcomings, especially with the poor wetting properties, and the heterogeneous surface charge, that result in adsorption of smaller molecules such as organic solvents (Monahan *et al.* 2002; Lee *et al.* 2003), fluorescent dyes (Lee *et al.* 2003; Abate *et al.* 2008), and proteins (Boxshall *et al.* 2006; Wong & Ho 2009), which leaves behind a foul surface. This effect was quite evident during surface characterization of the coated surfaces.

3.2 Impedance Analysis

Two devices, a) IviumStat - Electrochemical interface and impedance analyser, manufactured by Ivium Technologies, Eindhoven, Netherlands, and b)MEA-IT - Impedance testing device from Multi Channel Systems MCS GmbH, Reutlingen, Germany, are used in the measurement of the impedance.

3.2.1 Experimental Setup using IviumStat

The IviumStat principally comprises a microprocessor and a potentiostat or galvanostat, to control the potential or current applied to the electrodes, and to measure the response. The device is controlled through the IviumSoft software, and it operates on electrochemical sensors with a working electrode, sensing electrode, reference electrode, and an auxiliary or counter electrode. As a standalone device, it can be interfaced with the electrochemical cell through a 15 pin cell connector. However, in order to facilitate the connection to a MEA with several working electrodes, a multiplexer setup is used as shown in Figure 3.3.

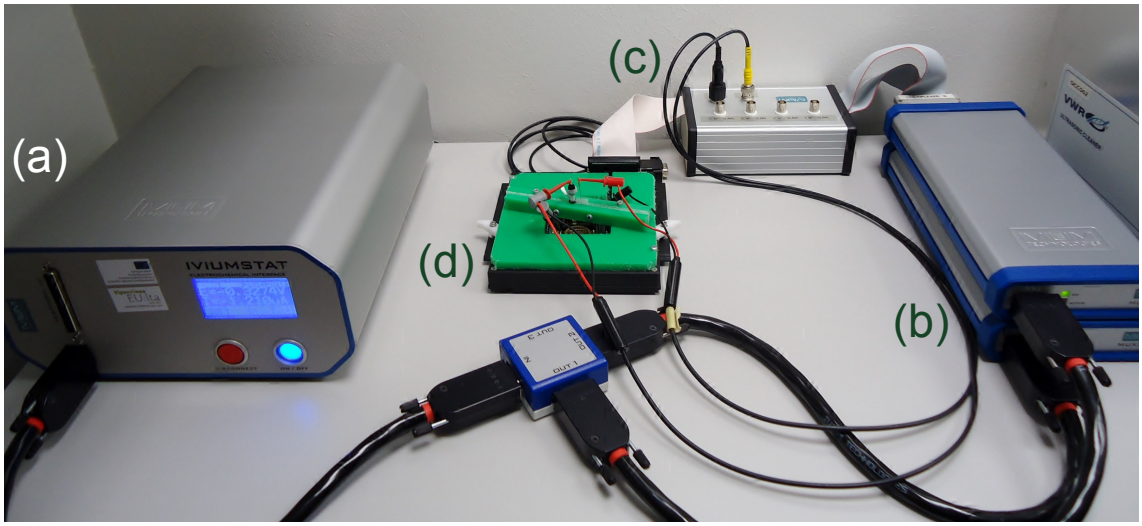

Figure 3.3: The experimental setup comprising the (a) IviumStat device, (b) Multi-WE32 modules, (c) break out box, and (d) MEA1060-INV adapter, that is used to measure the impedance of the MEA.

The IviumStat device is interfaced with the MEA1060-INV adapter (from Multi Channel Systems MCS GmbH, Reutlingen, Germany) through two Multi-WE32 modules, with 32 channels each, that are stacked together in order to measure 64 channels in all. The Multi-WE32 module, manufactured by Ivium Technologies, Eindhoven, Netherlands, partly performs the function of a multiplexer, in the sense that although potential or current is applied across all the channels simultaneously, output can be recorded from the channel of interest. The connection

between the Multi-WE32 modules and the MEA1060-INV adapter is established by means of a break out box, with a small computer system interface (SCSI) cable and two D-subminiatures with 37 contact pins (DC-37). Two additional Bayonet Neill-Concelman (BNC) connectors are used to provide connection to the reference and counter electrodes. Although the base plate and the MEA1060-INV adapter housing provide sufficient shielding, the open top of the adapter is closed with a custom made Faraday cage that is grounded to the adapter's housing, so as to prevent line-frequency interference.

3.2.2 Configuration of the Impedance Analyser

The measurement method and parameters such as applied potential or current, current range, frequency, operation mode etc., have to be configured before the measurements begin. A few of these parameters are discussed in detail below.

Measurement Method

A constant potential I-V method is employed, wherein the potential difference between the working electrode and the reference electrode is kept constant, and the corresponding current flowing through the circuit is measured. In implementing this method, a three electrode electrochemical setup with a reference electrode RE, counter electrode CE, and the working electrode WE is used as illustrated in the Figure 3.4.

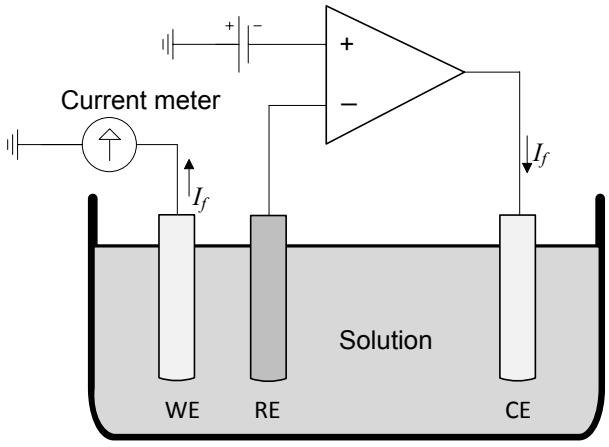

Figure 3.4: Concept diagram of a three electrode amperometric sensor and a potentiostat, as presented by Ahmadi & Jullien (2009).

The working electrode is maintained near ground potential through a control loop, and the instrument or the control amplifier forces a current through the counter electrode to maintain the potential at a constant value. The current flowing through the working electrode is measured, and the impedance is obtained as a ratio of

voltage to current. (IviumSoft User Manual 2010) A constant potential is maintained to ensure that the changes in electrode properties are not due to the change in potential (Aurien-Blajeni *et al.* 1989, cited in Weiland & Anderson 2000).

A silver/silver chloride glass electrode is used as the reference electrode, since it is non-toxic, inexpensive, and stable at relatively high temperatures. Owing to the inert nature, platinum wire electrode is employed as the counter electrode, and the MEA electrodes represent the working electrodes. Dulbecco's 0.0095 M phosphate buffered saline (PBS) without calcium and magnesium, from Lonza Group Ltd., Basel, Switzerland, is used as the buffer all through the experiment, except for those trials involving cells. PBS is utilised, as it is isotonic, and maintains a physiological pH range of 7.0 to 7.6, independent of the temperature.

Frequency

Based on experimental observations, and studies conducted by Weiland *et al.* (2002), the impedance amplitude of the titanium nitride electrode is found to be frequency dependant for frequencies less than 4 kHz. Therefore, the applied frequency is kept constant at 1 kHz, as it is the "fundamental action potential frequency often used to probe tissue properties around an implanted microelectrode" (Ludwig *et al.* 2006; Cogan 2008; Karp *et al.* 2008; Ward *et al.* 2009).

Current Range

Current range determines the current sensitivity during the experiment. In this case, the initial current range is set to 1 nA, and automatic current ranging is enabled in order to avoid overloads. This allows the instrument to determine the appropriate range. Although current overloads up to four times the current range may still render the correct measurement, it is unreliable. (IviumSoft User Manual 2010)

Noise Filtering

In order to minimize the impact of noise on impedance, analog filters are used in automatic noise filtering. Also, the acquisition time is altered suitably to obtain better filtering results. Increasing the measurement period enables the instrument to acquire more data points or cycles, which on averaging provide more accurate results. (IviumSoft User Manual 2010)

Operation Mode

Batch mode is employed in order to access the channels of the MultiWE32 module. The index variable of the module is set to loop, so as to measure the impedance from all 60 electrodes of the MEA. However, it is to be noted that, despite the

measurement being recorded from only one channel at a given instant, potential is applied across all the electrodes simultaneously. (IviumSoft User Manual 2010)

3.2.3 Setup and Configuration of MEA-IT

MEA-IT, manufactured by Multi Channel Systems MCS GmbH, Reutlingen, Germany is a portable impedance analyser designed specifically to measure the impedance of the MEAs. The device houses a 60 channel contact unit, and is connected to the computer via universal serial bus USB 2.0. The MEA whose impedance is to be measured is mounted on the device, and the measurement is controlled through the proprietary MEA-IT software. A silver/silver chloride pellet is used as the reference point for grounding the electrolyte bath and the MEA-IT system during measurements, as shown in Figure 3.5. The internal reference electrode(s) is/are measured just as any other electrode of the MEA, and thus external grounding is necessary to ensure the impedance values are not out of bounds. The device is configured by default to apply a 1 kHz sine wave of amplitude 100 mV, and the impedance is measured in units of kilo Ohm. (Impedance Testing Device, MEA-IT Manual 2012)

Figure 3.5: The MEA-IT device, with the MEA and the external reference electrode, as presented by Impedance Testing Device, MEA-IT Manual (2012).

3.2.4 Measurements

In general the impedance values are recorded using both the IviumStat and the MEA-IT devices, from the MEAs prior to coating, on coating, and subsequently after the removal of the coating. Before the commencement of the recording, the contact pads of the MEAs are cleaned with a soft tissue moistened with 70 % ethanol, in order to remove contaminations that may result in a poor contact between the pads and the amplifier pins.

Uncoated measurements are carried out merely with the buffer, following which the MEAs are coated as per the protocol established, and the measurements are performed again with the buffer. Although establishing a steady state is practically difficult, observations are made at a room temperature of 21 °C, and 24 hours after

the addition of the buffer. This is to minimize or rather standardise the effects of temperature changes, adsorption and/or build up of impurities and/or reagents in the solution, coating degradation etc. The coating is removed by soaking the MEA overnight in 1 % (w/v) Tergazyme^{TM} (manufactured by Alconox Inc., New York, USA) enzyme active powered detergent solution. The MEA is thoroughly washed with deionised water afterwards, and sterilised using 70 % ethanol before the start of the next experiment.

3.3 Noise Measurements

Noise measurements are made using the MEA2100 stand-alone system, distributed by Multi Channel Systems MCS GmbH, Reutlingen, Germany. It is used to acquire extracellular recordings from the MEA, and it principally comprises the MEA headstage with two 60 channel contact units, pre amplifier, filter amplifier with integrated data acquisition, and analog-to-digital converter. The headstage is interfaced to the computer through an interface board that houses the digital signal processor. The entire setup is shown in the Figure 3.6. The connection to the computer is established through an USB cable, and the data acquisition and analysis program, MC_Rack is used to record the noise signal. (MEA2100 - System Manual 2013)

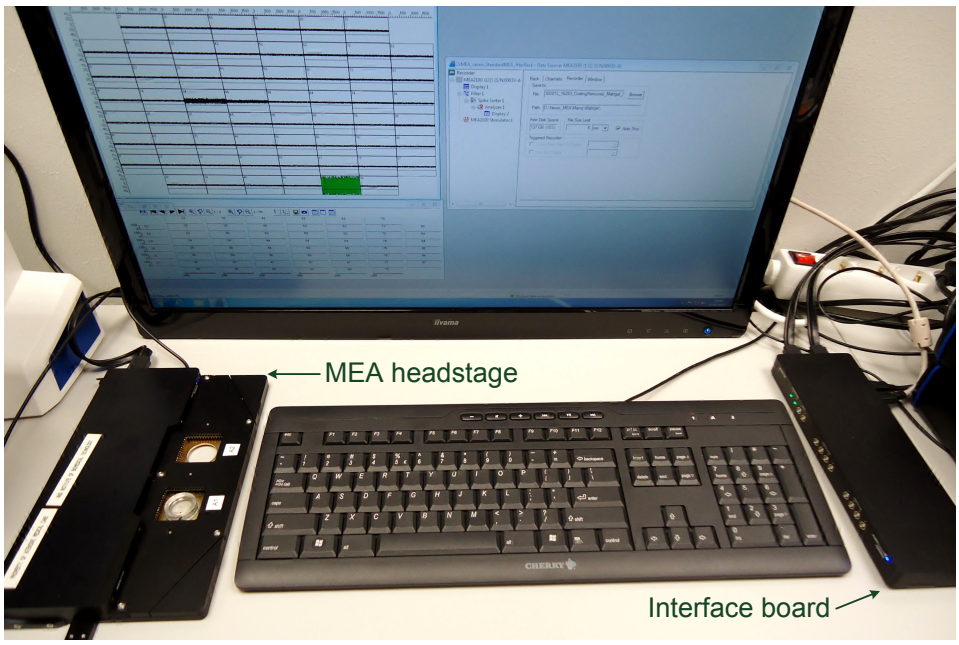

Figure 3.6: The measurement setup comprising the headstage and the interface board used to measure the noise from the MEA.

The noise values are recorded from the MEAs prior to coating, on coating, and subsequently after the removal of the coating. Before the start of the measurements though, the contact pads of the MEAs are cleaned with a soft tissue moistened with

70 % ethanol, so as to remove contaminations such as thin grease layer, that may result in a poor contact between the pads and the amplifier pins. Improper contact will in turn increase noise levels on the affected channel, inducing significant error in the recording.

Raw electrode data is obtained 24 hours after the addition of PBS, at a room temperature of 21 °C, and for a duration of 5 minutes. The sampling rate is set to 50,000 Hz. Although the base plate and the MEA amplifier housing provide sufficient shielding during the measurements, the open top of the amplifier is closed with a custom made Faraday cage, as a means to attenuate the line-frequency interference. The Faraday cage is grounded to the amplifier housing in order to dissipate the current generated by the electromagnetic fields. The RMS noise voltage is computed using the equation,

$$V_{rms} = \sqrt{\frac{1}{n_1}\sum_{i=1}^{n_1} {x_i}^2} \tag{3.1}$$

where n_1 represents the number of samples, and x_i is the amplitude of noise at the instant i. The computations are performed with MATLAB®, a high-level language for numerical computation and visualization, developed by The MathWorks Inc., Natick, USA.

3.4 MEA Coating Protocol

The protocol followed in the coating of the MEAs with the surface molecules such as a) Polyethyleneimine and laminin, b) gelatin, and c) Matrigel™ is discussed in this section.

3.4.1 Polyethyleneimine and Laminin

The pre-sterilised MEAs and the PDMS structures are washed thoroughly with 70 % ethanol, and are allowed to dry in the laminar flow chamber. Once dry, 1 ml of 0.05 % (w/v) PEI, distributed by Sigma-Aldrich Chemie GmbH, Schnelldorf, Germany, is added to each well, and the MEAs are incubated at 37 °C for two hours. A water bath is used to prevent the PEI from drying. Unbound PEI remaining in the well after incubation is removed, and the wells are washed with sterile water repeatedly for two to three times, so as to avert the high pH of the solution from adversely affecting the cells.

The MEAs are allowed to dry in a laminar flow cabinet, after which they are coated with 1 ml of laminin, obtained from Engelbreth-Holm-Swarm murine sarcoma basement membrane (supplied by Sigma-Aldrich Sweden AB, Stockholm, Sweden),

and diluted to a concentration of 20 μg/ml with Dulbecco's phosphate buffered saline containing no calcium and magnesium. The MEAs are placed in the incubator for two hours at a temperature of 37 °C. After incubation, unbound laminin is aspirated from the well.

3.4.2 Gelatin

The MEA, along with the PDMS structure that forms the well are washed thoroughly with 70 % ethanol, and dried in the laminar flow chamber. Once dry, 1 ml of 0.1 % Type A gelatin, obtained from porcine skin (from Sigma-Aldrich Chemie GmbH, Schnelldorf, Germany) is added to the well, and the MEA is incubated at 37 °C for an hour. A water bath is used to preclude the gelatin from drying, and unbound gelatin remaining in the well after incubation is removed.

3.4.3 Matrigel™

Matrigel™ basement membrane matrix with reduced growth factor, distributed by BD Biosciences - Discovery Labware, Billerica, USA, is used for coating the MEAs. Two different procedures are adopted here a) thin gel method, often used for plating cells on top of the gel, and b) thin coating method, employed for growing cells on the surface of the complex protein layer. Before proceeding with the coating, Matrigel™ is thawed in ice at a temperature of 4 °C, for an interval of 2 hours or until it liquefies. The pipette tips, and the fulcan tubes are cooled to around 4 °C prior to use, as Matrigel™ solidifies at temperatures around 10 °C (Matrigel™: Guidelines for use 2012).

Thin Gel Method

The MEA together with the PDMS structure is rinsed thoroughly with 70 % ethanol, and dried in a laminar flow chamber. About 50 μl/cm^2 of Matrigel™ is added to the well, and the MEA is incubated at a temperature of 37 °C for 30 minutes. A water bath is used to forestall the Matrigel™ from drying. Unbound Matrigel™ is aspirated from the well after incubation, and the MEA is gently rinsed with serum-free medium. (Matrigel™: Guidelines for use 2012)

Thin Coating Method

The MEA together with the PDMS structure is rinsed thoroughly with 70 % ethanol, and dried in a laminar flow chamber. Matrigel™ is diluted to one-tenth of its concentration using Dulbecco's modified eagle medium containing Ham's nutrient mixture F-12 (Gibco® DMEM/F-12, produced by Invitrogen Corporation, Paisley,

Scotland) in a 1:1 ratio. The medium is devoid of lipids, proteins and/or growth factors. The extensively diluted Matrigel^{TM} is then added to the well, in a quantity sufficient enough to cover the electrode area. The MEA is incubated at a temperature of 37 °C for 30 minutes. A water bath is used to prevent the Matrigel^{TM} from drying. Unbound Matrigel^{TM} remaining in the well after incubation is removed, and the MEA is gently rinsed with the culture media.

3.5 Experiment with Cells

The influence of the cells on the overall impedance, and noise of the MEA is analysed after plating neural cells on the MEA substrate. The various processes involved in the dissociation, plating, and imaging of the cells are explained in detail below.

Dissociation of the Cell Aggregates

The cell aggregates growing in the suspension are collected in an Eppendorf tube and cell dissociation enzyme Tryple^{TM} is added to the aggregates, in proportions equivalent to 500 μl for the cell mass of one well of the 6 well plate. They are then incubated at a temperature of 37 °C for a maximum interval of 15 minutes, with intermittent back and forth pipetting of the aggregates. After incubation, the aggregates are broken down into forming a single cell suspension, by pipetting the medium along the inner wall of the tube. Zero NDM is then added to the Eppendorf tube in quantities ten times to that of Tryple^{TM}, and the tube is centrifuged at a speed of 1500 rpm for five minutes. The medium is then replaced, and the centrifugation process is carried out again. After the cleaning procedure is complete, fresh media is added to requirement and the cells are counted using the Bürker cell counter.

Cell Plating

The 6 well MEA plate together with the PDMS structure that isolates the electrodes, is autoclaved and sterilised with 70 % ethanol, before being treated with PEI and laminin as per the protocol discussed earlier. After coating, the cell aggregates are added to the MEAs, and incubated at a temperature of 37 °C, with an atmospheric carbon-dioxide level of 5 %. Once the aggregates have attached, the medium devoid of basic fibroblast growth factor is substituted with medium containing both the fibroblast growth factor and the brain derived neurotrophic factor.

Measurements

Approximately 68 hours after cell plating, the MEAs are removed from the incubator and are allowed to cool down to a room temperature of 21 °C. The noise measure-

ments are carried out thereafter, and the MEAs are returned to the incubator. This is done so as to preclude prolonged exposure of the cells to unfavourable environmental conditions, which might destroy them. After a period of 15 to 30 minutes, the MEAs are removed from the incubator, and the impedance measurements are performed at room temperature.

Imaging

The positioning of the cells against the MEA plate is imaged using an optical microscope. The viability of the cells on the other hand, is analysed with the LIVE/DEAD® Viability/Cytotoxicity Kit for the mammalian cells, from Molecular Probes Inc., Eugene, USA. About 0.5 μM of Ethidium homodimer-1, and 0.1 μM of Calcein-AM are added to the cells along with the cell culturing medium. The MEAs are incubated for a period of 30 minutes, and then viewed with a immunofluorescence microscope, Olympus IX51, manufactured by Olympus Soft Imaging Solutions GmbH, Münster, Germany.

In case of dead cells, Ethidium homodimer-1 penetrates the disrupted cell membrane and binds to the nucleic acids, a process that enhances its fluorescence by 40 fold with a bright red emission at 568 nm. On the contrary, Calcein-AM is retained within live cells, and the intracellular esterase activity renders the Calcein-AM fluorescent, thereby emitting a green fluorescence at a wavelength of 515 nm. The background noise is reduced in either case, since both the dyes are non-fluorescent prior to their interaction with the cells. (Product Information: LIVE/DEAD® Viability/Cytotoxicity Kit 2005)

The images are obtained with the Olympus DP71 camera, produced by Olympus Soft Imaging Solutions GmbH, Münster, Germany. Further image enhancement is performed with Adobe Photoshop CS4, a digital imaging software distributed by Adobe Systems Inc., San Jose, USA.

3.6 Evaluation of the Coating Thickness

The thickness of the coating is measured using DektakXT™ stylus profilometer, manufactured by Bruker Corporation, Tucson, USA. The profiler employs a stylus that operates based on contact method for surface characterization. A proportional-integral-derivative servo controller suspends the stylus in a free floating state, thereby maintaining constant force over long intervals. The surface features of the sample as encountered by the stylus, are obtained in real time as a two dimensional profile, and further processing is carried out using the data analyser. The device and the measurements are controlled through the operation and analysis software, Vision64. (Dektak XT Stylus Profiler - User Manual 2011)

3.6.1 Configuration of the Stylus Profilometer

Before the measurement is initiated, the 'X-Y' co-ordinates of the stage and the 'Theta' or the angular orientation of the stage assembly are initialised, and the basic device parameters such as scan type, range, profile, stylus type, stylus force, length, resolution, etc. are pre-set as briefed below.

Scan Type: The thickness measurements are not performed relative to one another, and hence a standard scan mode is chosen, wherein the scan is executed across the sample surface, and the tower is reset before the start of the subsequent scan. In other words, the measurements are made over the length of the sample, and every successive scan has its own reference point. (Dektak XT Stylus Profiler - User Manual 2011)

Range: Besides determining the operating range, 'Range' also defines the vertical resolution of the scan. Since the surface texture of the sample includes very fine structures, an operating range of 6.5 μm is chosen in most cases, which offers a vertical resolution of 0.1 nm approximately. For measurements involving the thick Matrigel^{TM} coating though, the operating range is increased to 65.5 μm, in order to prevent 'topping out' or 'bottoming out' of the trace. The vertical bit resolution in this case is reduced to 1 nm. (Dektak XT Stylus Profiler - User Manual 2011)

Profile: Profile represents the surface characteristics of the sample to be measured. Since the characteristics of the coatings are not well established, 'Hills and Valleys' mode is applied, which halves the measurement range into expanses above and below the horizontal line. (Dektak XT Stylus Profiler - User Manual 2011)

Stylus Type: A stylus with 2 μm tip radius, etched or milled from a diamond stock is utilised to determine the surface texture. (Dektak XT Stylus Profiler - User Manual 2011)

Stylus Force: A low force of 0.5 mg or 0.75 mg as required to establish contact with the surface, is applied to the stylus in safe mode. This mode reduces tip drag during touchdown, and is optimised to protect the force-sensitive samples. (Dektak XT Stylus Profiler - User Manual 2011)

Length: The scan length is appropriately chosen so that the trace forms a secant line to the coated surface. (Dektak XT Stylus Profiler - User Manual 2011)

Resolution: The horizontal resolution, which in this case represents the horizontal distance between two data points, is varied over the range of 0.004 to 0.062 μm/sample, depending on the length of the measured surface. This variation in the resolution is due to the limitation in the number of data points that the system is designed to acquire during a measurement. (Dektak XT Stylus Profiler - User Manual 2011)

3.6.2 Measurements

Microscopic slides are employed as substrates for the thickness measurements of the MEA coatings. The glass surface is wiped clean with a tissue moistened with 70 % ethanol, and the protein coatings are formed over a small surface of the microscopic slide following the protocol described earlier. The coated surface is laterally exposed to compressed air stream, so as to remove any unbound material and/or residual liquids from the surface. In order to preserve the characteristics and the texture of the coating, the slides are coated a few hours or minutes before the commencement of the measurement. However, the slides are air dried before being placed in the profiler for measurement, so as to prevent the wet sample from defiling the stylus.

The profiler is placed over a vibration isolation table, and is allowed to stabilize for approximately 15 to 30 minutes before the start of the measurements, as the system is sensitive to transient convective flow. An acrylic enclosure is utilised to protect the entire setup from the external environmental factors such as noise, air currents, and dust. (Dektak XT Stylus Profiler - User Manual 2011)

The sample is mounted on the measurement stage of the profiler, and is held in place by a vacuum chuck. The X-Y position of the motorised stage is adjusted so as to position the area of the interest on the sample under the stylus. Also the orientation of the sample with respect to the stylus, given by 'theta' is altered suitably, and the measurements are made along the secant line of the coated surface as represented in Figure 3.7. The sample positioning stage is levelled manually whenever necessary, in order to obtain a better profiler performance and to prevent the saturation of the trace.

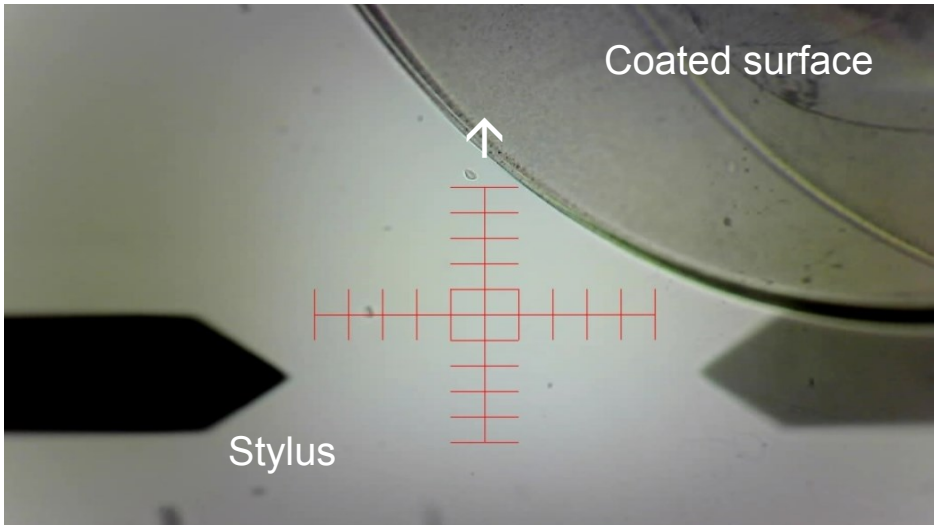

Figure 3.7: This image taken prior to the measurement captures the initial position of the stylus.

Data Processing

The surface trace obtained from the live measurement is levelled using the Vision64 software. The raw data in the data analyser is initially pre filtered by the tilt removal filter, after which a two point linear fit is applied, which re-plots the trace and levels with the cursor intercepts at zero.

3.7 Evaluation of the Surface Roughness

Surface characterization is performed using an atomic force microscope, XE-100, manufactured by Park Systems Corp., Suwon, South Korea. The device employs multi-purpose silicon cantilevers with pyramidal tips, marketed as 'ACTA' by Applied NanoStructures Inc., Santa Clara, USA, and is enclosed in an environmentally sealed acoustic chamber, to shield from the external acoustic and light noise. Measurements and user control of the atomic force microscope is acquired using the data acquisition program XEP. Quantitative analysis, and further image processing is carried out using the proprietary software XEI.

3.7.1 Configuration of the Atomic Force Microscope

Similar to the other measurement devices, the atomic force microscope is to be configured as well, before the start of the measurements. Some of these parameters such as the mode of operation, voltage modes, Z scanner range, fast scan axis, scan direction, scan size, scan rate, and Z servo gain are briefed below.

Head Mode: Intermittent contact mode is chosen, as it minimizes the effect of friction and other lateral forces (Bhushan 2008).

Voltage Modes: The X-Y scanner, and the Z scanner are operated at high voltage modes, so as to force the scanner to its maximum limit and enable the investigation of a wide range of structures. (XE-100 : High Accuracy Small Sample SPM 2002)

Z Scanner Range: The range that can be varied from 0 to 1 is set to 0.5, a numerical value corresponding to 6 μm range of the Z scanner in high voltage mode. This reduction in the range offers an increased vertical resolution of 10 Å. (XE-100 : High Accuracy Small Sample SPM 2002)

Scan Size: The size of the scan area along the X and the Y axis is set to 2 μm each. In other terms, the effective scan area is 2 μm $\times$ 2 μm. (XE-100 : High Accuracy Small Sample SPM 2002)

Scan Rate: The scan rate or the frequency at which the scanner rasters back and forth the sample surface is set to 1 Hz. (XE-100 : High Accuracy Small Sample SPM 2002)

Z Servo Gain: It represents the sensitivity of the Z scanner feedback loop. A high value may result in oscillations, and in effect an increased noise level in the image. Conversely, a very low gain will result in improper surface tracking. Hence the servo gain is adjusted suitably so that the oscillations are reduced, and the line trace is stabilised. (XE-100 : High Accuracy Small Sample SPM 2002)

3.7.2 Measurements

Three different 6 well MEAs, an uncoated MEA, a MEA coated with PEI, and another treated with both PEI and laminin were used in the surface roughness measurements. The MEAs are coated a few hours in advance to the measurements, and as per the protocol established previously. The air dried MEAs are placed in the atomic force microscope, and the surface roughness over an area of 2 μm $\times$ 2 μm of the reference electrode, the silicon nitride coated titanium track, and the silicon nitride covered glass surface is obtained as a TIFF data file. These surfaces are chosen in particular, as it is the titanium nitride electrode(s) and the silicon nitride insulation that primarily influence the impedance of the MEA. The reference electrodes are preferred over the microelectrodes as they have a relatively

large surface area, and are expendable if at all any untoward incident were to occur during the measurements.

Data Processing

The data is flattened to eliminate the slopes and the curvature generated by the scanning procedure, as these artefacts influence on the height data and render the image difficult to interpret. A fitting curve or an estimation of the curvature and/or slope, determined by polynomial regression is employed along the vertical and horizontal axes to flatten the image as illustrated in Figure 3.8. A 3D image of the surface is then rendered from this flattened image using suitable parameters. (XEI: Powerful Image Processing Tool for SPM Data 2008)

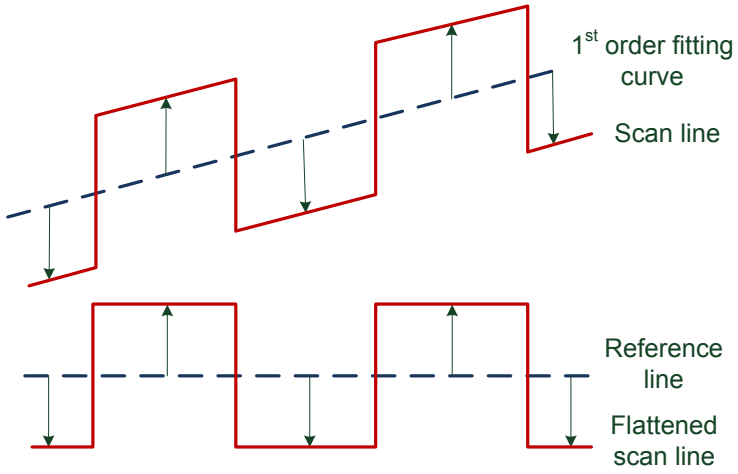

Figure 3.8: An example of flattening applied to a single line in one dimension. (XEI: Powerful Image Processing Tool for SPM Data 2008)

3.8 Estimation of Molecular Adsorption

The molecular adsorption of PEI and laminin is studied using SPR Navi^{TM} 210A-3L device, manufactured by Bionavis Oy Ltd., Ylöjärvi, Finland. It is an optical prism coupler based SPR sensor, that functions based on Kretschmann's configuration. The device principally comprises a) the opto-electronic section that includes the lasers, optical prism and the control electronics, b) the docking station for the sensor slides, and c) the fluidic segment consisting of the flow cells, injection ports and the associated tubing. (SPR-Navi 210A User Manual 2012)

The device measures the angle at which resonance occurs, a variable that is sensitive to the change in the refractive index of the medium adjacent to the sensor slide interface, by recording the intensity of the reflected beam as the system ventures out of resonance. As resonance is approached, a drop in the intensity of the reflected light is evidenced due to the excitation of the plasmons, as illustrated in Figure 3.9.

The equipment is interfaced with the computer through an USB cable, and the measurements are handled with the SPR Navi^{TM} software. However, the change in the SPR angle corresponding to the molecular adsorption on the sensor slide is obtained from the SPR Navi^{TM} Data Viewer. (SPR-Navi 210A User Manual 2012)

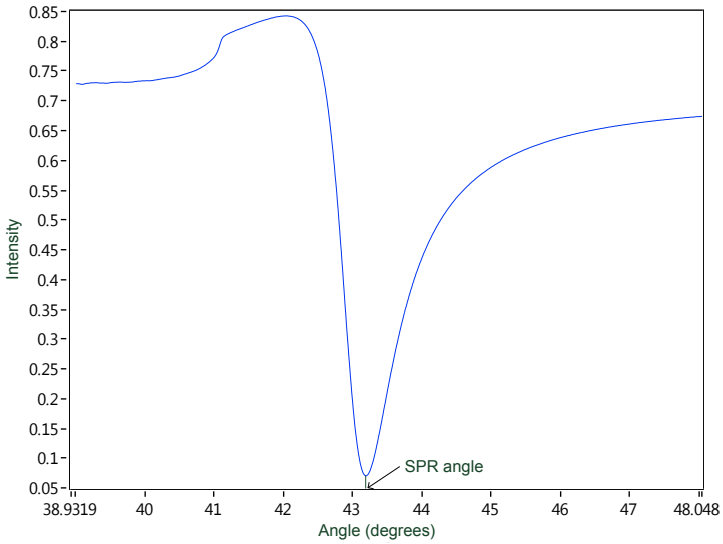

Figure 3.9: A representation of the resonance curve measured using the SPR Navi^{TM} 210A-3L device.

3.8.1 Configuration of the SPR Device

The SPR device parameters such as the laser wavelength, measurement method, and the chamber temperature are configured before the start of the measurement as detailed below.

Laser Wavelengths: Two different incident light wavelengths at 670 nm and 785 nm are employed for the measurements.

Measurement Method: An angular scan is performed over the full range of the equipment from 38 ° to 78 °, wherein the prism is turned against the laser beam and the entire resonance curve is recorded. (SPR-Navi Software Manual 2012)

Temperature: The measurement chamber, including the prism, and the electrochemical flow cell are maintained at a temperature of 37 °C.

3.8.2 Measurements

Two different sets of measurements are performed a) to estimate the differential adsorption of laminin to PEI with varying concentrations of laminin such as 20 μg/ml, 40 μg/ml, and 80 μg/ml, and b) to study the kinetics of the reaction.

Differential Adsorption of Laminin

SPR Navi^{TM} gold sensor slides SPR102-AU of dimension 12 × 20 mm, distributed by Bionavis Oy Ltd., Ylöjärvi, Finland, are employed as substrates for coating. The SPR angle of the uncoated slide is measured initially in air medium, after which the gold surface of the slide is coated with PEI, followed by laminin shortly thereafter, and the corresponding changes in the SPR angles are recorded.

The coatings are formed elsewhere, away from the SPR device, and as per the protocol established earlier. The slides are allowed to dry before they are mounted back on the dock, so as to prevent any residual liquid droplets from influencing the measurement. The measurements are repeated with varying concentrations of laminin such as 20 μg/ml, 40 μg/ml, and 80 μg/ml, and their respective SPR angles are measured.

The coated slides are cleaned by soaking them overnight in 1 % (w/v) Tergazyme^{TM} detergent solution. It is rinsed with deionised water afterwards, and air dried in a clean environment before the start of the successive experimental trial. The glass surface of the sensor is maintained immaculate, as otherwise, it may lead to erroneous observations, besides befouling the optical elastomer that couples the prism with the sensor slide. When required, the slide is gently wiped using a low lint tissue moistened with acetone.

Kinetics Study

Kinetics study is similar in approach to the differential adsorption experiments, but unlike the previous method, the coating is made *in situ* and the measurement is continuous over the entire period. After the initial SPR measurement with the bare gold slide in air medium, PEI solution is slowly injected into the flow cell and the change in the SPR angle over time is observed. An electrochemical flow-cell SPR321-EC made of polyetheretherketone and distributed by Bionavis Oy Ltd., Ylöjärvi, Finland, is utilised to hold the sample of volume 100 μl. After an hour, PEI is drawn out and sterile water is infused into the flow cell to rinse off unbound PEI from the measurement chamber. The slide is left to dry, while the SPR angle in air medium is recorded. Laminin is slowly forced in thenceforth, until the flow cell is completely filled. Laminin is extracted from the measurement chamber after an interval of two hours, and the SPR angle in air medium is examined.

Care is taken so as to not introduce air bubbles in the flow cell. In addition, the solution is degassed and warmed to a temperature of 37 °C prior to the injection, in order to prevent sudden changes in temperature.

4. RESULTS AND DISCUSSION

4.1 Impedance and Noise Measurements

The changes in the electrode impedance and the RMS noise magnitudes of the MEA, upon coating with suitable surface molecules such as PEI and laminin, gelatin, and Matrigel^{TM} are examined, and the outcomes of this study are presented below.

4.1.1 PEI and Laminin

The differences in the impedances of the electrodes before and after coating the 6 well MEA with PEI and laminin are illustrated in Figure 4.1. A few electrodes exhibit a significant gain in the impedance on coating with PEI and laminin. However this trend is not universal as a sizeable amount of electrodes display either no change or a very moderate modification in this regard. The differences in the impedance values could partly be attributed to the random adsorption of the surplus laminin remaining in the well, and the constituents of the culture media. Nevertheless, the results are concurrent with the findings of He & Bellamkonda (2004), where no significant difference in the electrode impedances of the silicon MEA is reported with the addition of PEI and laminin.

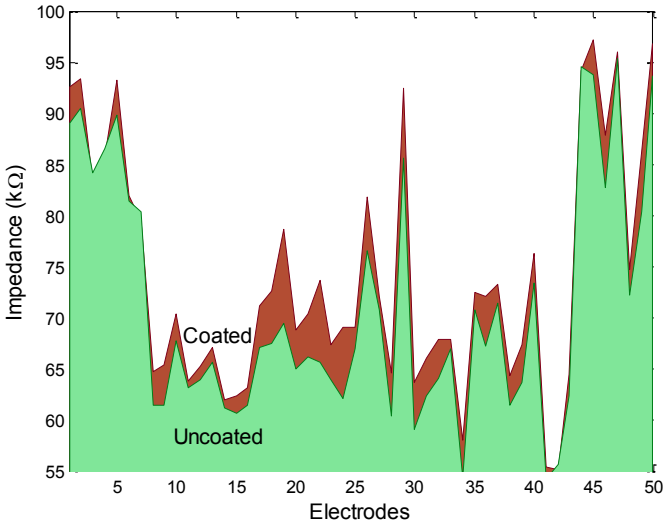

Figure 4.1: The changes in the electrode impedances, recorded from one of the four MEAs used in the experiment, before and after coating with PEI and laminin.

The average RMS noise amplitudes of the MEA electrodes remained almost the same at 2.35 μV, as against the 2.31 μV obtained prior to coating. It is to be noted that no external shield was used in this case to isolate the experimental setup from external electromagnetic interference, and chances are that the external interferences overwhelmed the recordings. The effect of shielding on the overall noise measurement is illustrated in Figure 4.2.

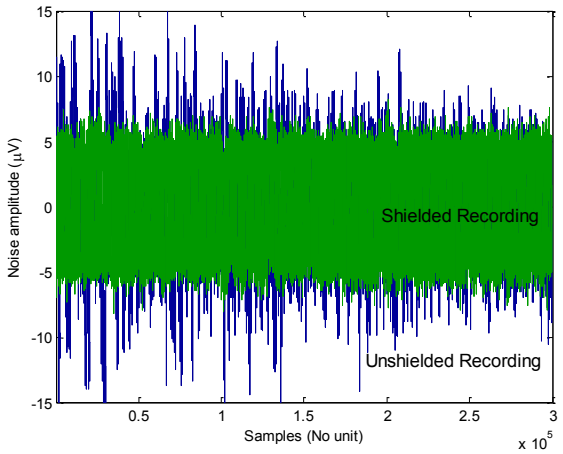

Figure 4.2: The effect of shielding on the overall noise measured from the MEA. The unshielded recording is represented in blue, whereas the shielded measurement is presented in green.

The difference may not appear significant on visual interpretation, but when the average RMS noise amplitudes are determined, the values more than halved with shielding in a few instances. An overview of the average RMS noise magnitudes of the 6 well MEA is presented alongside the electrode impedances in Table 4.1.

Table 4.1: Differences in the impedance and the RMS noise amplitudes of the MEA electrodes, with the addition of PEI and laminin.

MEA Status	**Average RMS Noise (μV)**	**RMS Noise Deviation (μV)**	**Average Impedance Magnitude (kΩ)**	**Impedance Magnitude Deviation (kΩ)**
Uncoated	2.31	0.15	71.05	11.66
Coated	2.35	0.16	73.41	10.96

4.1.2 Gelatin

The impedances of the standard 8 $\times$ 8 MEA electrodes show a modest increase in magnitude after coating with gelatin, as plotted in Figure 4.3. The changes are

not consistent and a few electrodes exhibit higher impedances which could partially be due to random adsorption of excess gelatin remaining in the well after coating. Although unbound gelatin was aspirated using a pipette, only so much could be removed without unsettling the coating. No significant changes were determined with respect to the RMS noise voltages measured prior to coating.

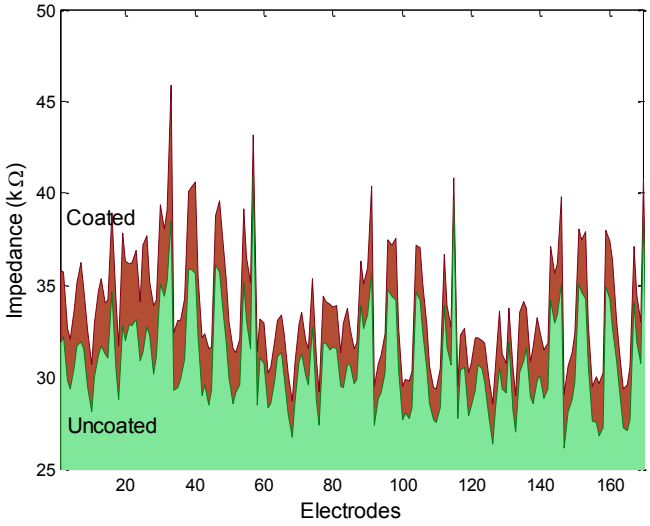

Figure 4.3: The electrode impedances prior to coating are presented in green, while the corresponding MEA impedances after coating with gelatin are coloured red.

No previous studies could be traced for direct comparison of the results. The summary of the average impedances and the RMS noise magnitudes, along with the respective standard deviations observed between the MEA electrodes is provided in Table 4.2. It can be observed that the overall noise and the impedance amplitudes of the MEA drop after the coating is removed. This drift is realised all throughout the study and will be discussed later.

Table 4.2: Differences in the impedance and the RMS noise amplitudes of the MEA electrodes with the addition of gelatin.

MEA Status	**Average RMS Noise (μV)**	**RMS Noise Deviation (μV)**	**Average Impedance Magnitude (kΩ)**	**Impedance Magnitude Deviation (kΩ)**
Uncoated	1.71	0.08	30.10	1.94
Coated	1.70	0.07	32.77	2.37
Coating removed	1.68	0.08	29.23	1.95

4.1.3 Matrigel™

The differences in the average impedance and RMS noise magnitudes of the standard 8×8 MEA electrodes, on coating with Matrigel™, employing both the thin coating and the methods are discussed below.

Thin Coating Method

A notable change of about 6 kΩ in impedance is observed after the MEA was exposed to a thin coating of Matrigel™ as illustrated in Figure 4.4. A few variations in the trend is discovered, similar to those noticed with the gelatin coating, partly due to the differential adsorption of Matrigel™ to the MEA surface.

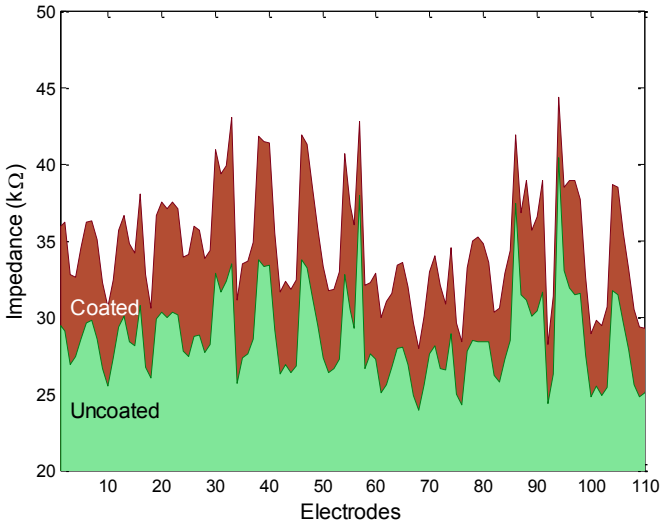

Figure 4.4: The variations in the impedances of the uncoated MEA electrodes are presented in green, and the respective changes in their impedances subsequent to the treatment with a thin coating of Matrigel™, are represented in red.

The average RMS noise amplitude of the MEA displays a mild increment with the addition of the thin Matrigel™ coating as given in the Table 4.3. No previous reports could be found from the comprehensive search, for direct comparison of the results.

Table 4.3: The effect of the thin coating of Matrigel^{TM} on the impedance and the RMS noise magnitudes of the MEA.

MEA Status	Average RMS Noise (μV)	RMS Noise Deviation (μV)	Average Impedance Magnitude (kΩ)	Impedance Magnitude Deviation (kΩ)
Uncoated	1.67	0.05	27.69	1.59
Coated	1.73	0.09	33.43	2.27
Coating removed	1.66	0.05	27.30	1.66

Thin Gel Method

On coating a thin gel of Matrigel^{TM} upon the MEA, an average increment of approximately 10 kΩ is recorded in the impedance magnitude of the electrodes, as represented in the Figure 4.5.

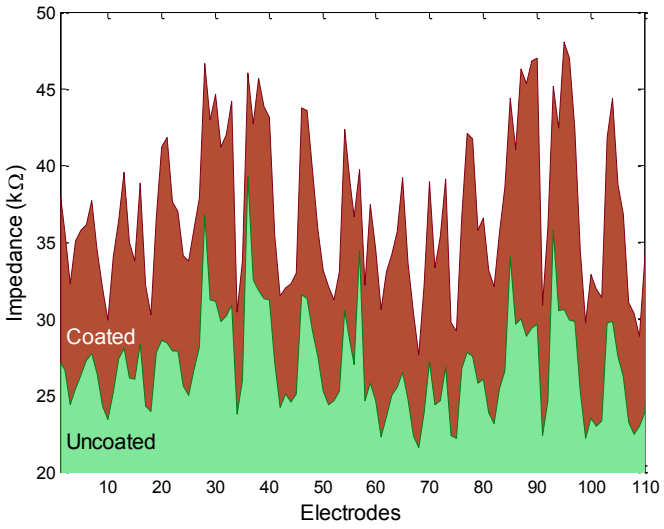

Figure 4.5: The changes in the electrode impedances prior to coating are presented in green, and the corresponding MEA impedances after coating with Matrigel^{TM} are displayed in red.

The average RMS noise values of the MEA electrodes show a moderate increase, similar to that exhibited by the thin coating method. The impedance and the noise magnitudes, along with the corresponding standard deviations observed between the electrodes are presented in Table 4.4. However no previous reports could be acquired from the comprehensive search, for direct comparison of the results.

Table 4.4: Differences in the impedance and the RMS noise magnitudes of the MEA, with the addition of a thin gel of Matrigel^{TM}.

MEA Status	**Average RMS Noise (μV)**	**RMS Noise Deviation (μV)**	**Average Impedance Magnitude (kΩ)**	**Impedance Magnitude Deviation (kΩ)**
Uncoated	1.65	0.05	26.50	2.13
Coated	1.73	0.05	36.61	4.31
Coating removed	1.65	0.06	26.04	2.28

As the experiments progressed, the wear on the electrodes was evident from the impedance measurements. The impedance of the standard 8 $\times$ 8 MEA decreased with every subsequent experiment as illustrated in the Figure 4.6, which could have impacted the measurement outcomes. This drift in impedance could be attributed to the degradation of the silicon nitride insulation layer that isolates the electrodes, resulting in an increase in the effective surface area and a corresponding decrease in the impedance of the electrodes.

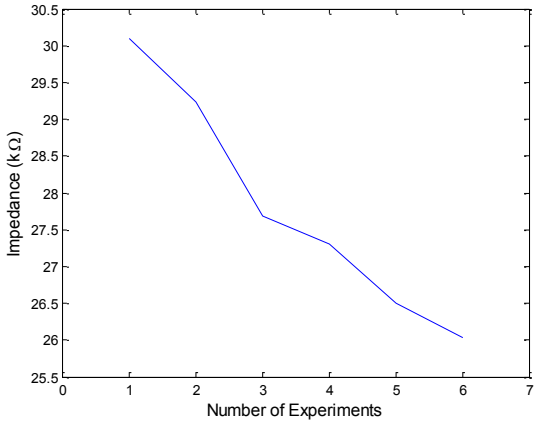

Figure 4.6: The drift in the overall impedance of the MEA, as the measurements progressed forward.

4.2 Measurements with Cells

The changes to the electrode impedances and noise are studied as the 6 well MEAs are plated with neural cells, and the end results of these experiments are detailed in this section.

Imaging

The viability of the cells plated on top of the 6 well MEAs is analysed with the LIVE/DEAD® Viability/Cytotoxicity Kit for the mammalian cells, and the images obtained using the immunofluorescence microscope is presented in Figure 4.7.

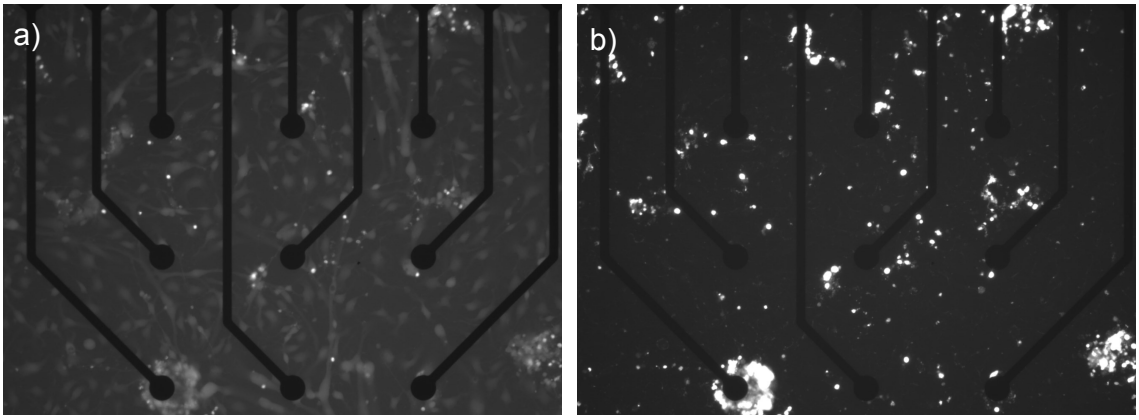

Figure 4.7: The fluorescence images acquired from the live cells plated over one of the six MEA wells, is presented in (a), and the bright spots in (b) represent the dead cells present alongside the live ones.

For further clarity, the two images in the Figure 4.7 were superimposed and enhanced using Adobe Photoshop CS4, whereby the live cells were illuminated green, while the dead ones were coloured red, as shown in the Figure 4.8.

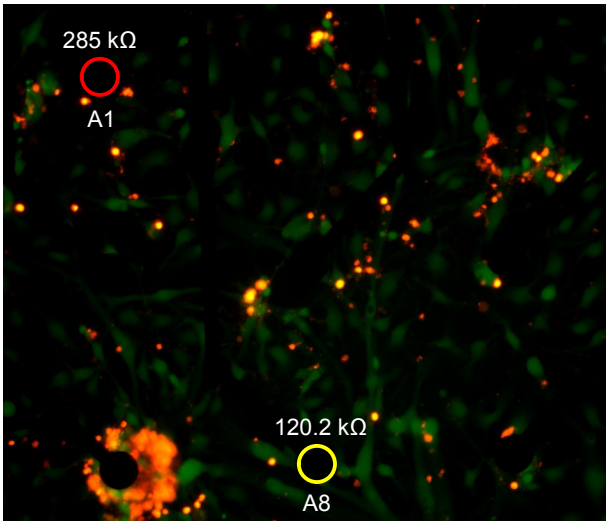

Figure 4.8: The enhanced fluorescence image, wherein the live cells are presented in green, and the bright red spots represent the dead cells.

Impedance and Noise Measurements

The addition of cells to the coated MEA surface brings about drastic variations in the electrode impedances, ranging from 75 kΩ to 350 kΩ, possibly corresponding to

the differences in the position and the orientation of the cell(s) over the electrode surface. Similar to the impedance measurements, a significant difference in the RMS noise voltage was observed between the cell plated MEA electrodes, varying from as low as 4 μV to upto 13 μV.

Nevertheless no particular conclusion could be reached, as the field of view was obscured by the MEA electrodes. Although the fluorescence images reveal the overall distribution of the cells over the MEA surface, cells lying on top of the opaque electrode surface could not be imaged from the bottom, rendering it difficult to relate the change in the impedance and the noise magnitudes to the positioning of the cells atop the MEA electrodes. For instance, the electrode A8, surrounded by the yellow ring in Figure 4.8 recorded the lowest impedance of 120.2 kΩ amongst the electrodes in the well, despite appearing to have been besieged by cells. On the other hand, the electrode A1, enclosed in the red circle and barely displaying any perceptible indication of a cell overhead or at close proximity in Figure 4.8, presented the highest impedance of 286.5 kΩ in the well, effectively illustrating the uncertainties surrounding the positioning of the cells.

4.3 Thickness Measurements

The results obtained from the thickness measurements of the a) PEI and laminin, b) gelatin, and c) Matrigel^{TM} coatings, conducted using the stylus profilometer are elaborated below.

4.3.1 PEI and Laminin

The nano scale coating thickness of PEI and laminin could not be reliably measured owing to the inherent surface variations of the coated substrate, and the residual material atop the coated surface. The profiler output representing the surface variations of the coating is presented in Figure 4.9. The observed divergence ranged from a few nanometres to tens of nanometres.

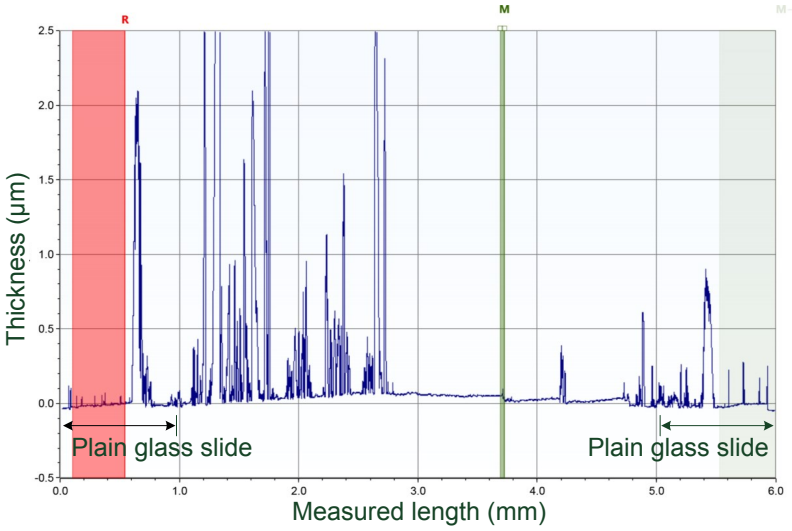

Figure 4.9: The surface trace of the PEI and laminin coating as obtained from the profiler. Approximately 1 mm from the start and the end of the trace is plain glass surface.

PDMS structures were utilised to contain the coating material over the MEAs. However no such structures are used with the microscopic glass slides for the thickness measurements, as molecular adsorption to the PDMS structure befouled the substrate as imaged in Figure 4.10. This crippled the possibilities of restricting the coated surface area and rendered the measurements vulnerable to the inherent surface variations of the slide.

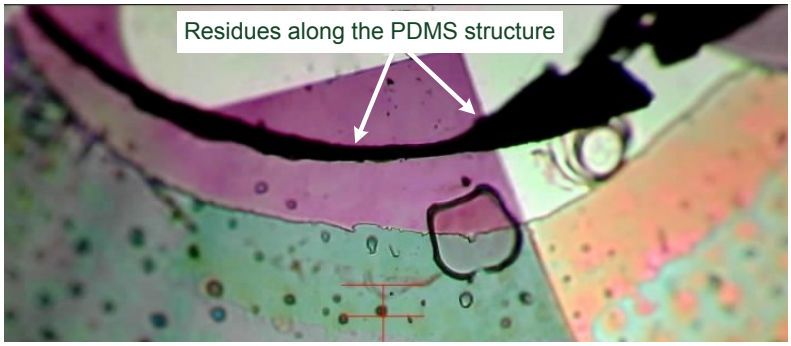

Figure 4.10: The residues along the PDMS structure, left behind after treating the surface with PEI and laminin.

Also, as the coated surface was allowed to dry, PBS, originally used to dilute laminin to the desired concentration, formed 'rock-salt' like crystal structures, that hindered the measurements and were recorded as spikes in the trace. The coated surface was exposed to a stream of compressed air in hopes of eliminating the salt residues, however a few random spikes still continued to persist even after the exposure.

Besides, external factors, and the limitations of the profiler could have also introduced uncertainties in the measurement. Although the profiler offers a high vertical resolution of 0.1 nm, or 1 nm depending on the range, the diameter of the stylus tip used is 4 μm, and surface features such as high aspect ratio trenches that are less than and/or approximately the same size may not have been realized at the output.

4.3.2 Gelatin

The measurements involving the gelatin coating endured the same impediments as that of the PEI and laminin coating, and the attempts to measure the coating thickness were futile. The trace obtained from the profilometer is pictured in the Figure 4.11.

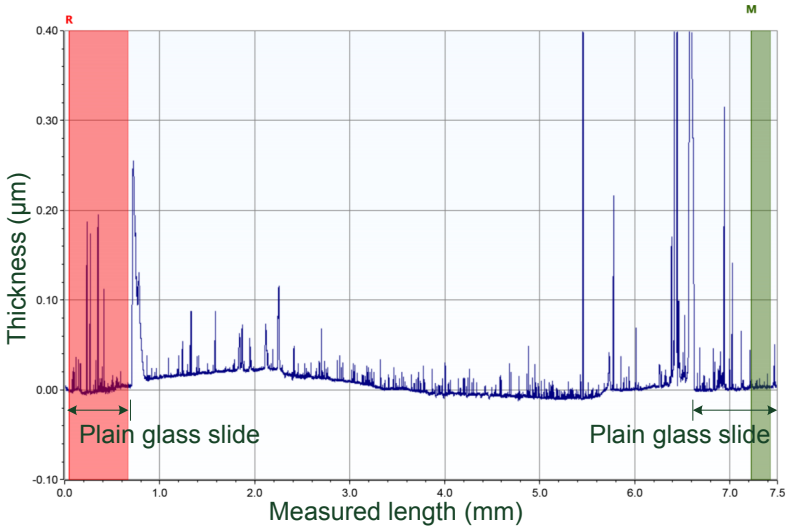

Figure 4.11: The surface variations across the gelatin coated surface as recorded from the profiler. Approximately 1 mm from the start and the end of the trace is plain glass surface.

4.3.3 Matrigel™

The thickness of the Matrigel™ coating has been evaluated using the profilometer, and as expected the differences in the thickness between the thin coating method, and the thin gel method were evident.

Thin Coating Method

In thin coating method, Matrigel™ is diluted using culture media and the coated surface is rinsed with the same, before the coating is allowed to dry. This medium however leaves a residue over the coated surface as it dries which was distinctly observed during the measurements, as in the Figure 4.12.

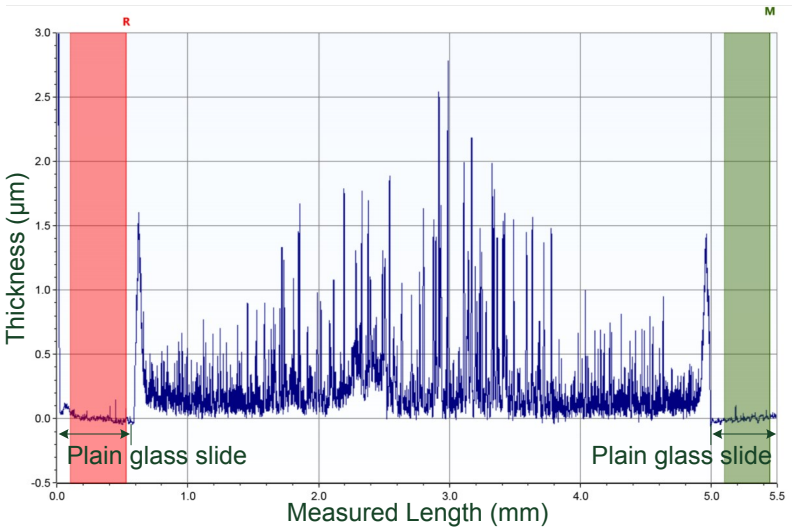

Figure 4.12: The fluctuations along the Matrigel^{TM} coated surface, observed with the profilometer. About 0.2 mm from the start and the end of the trace is plain glass surface.

When compressed air was used to eliminate the residual material, the spikes diminished and the thickness of the Matrigel^{TM}in the thin coating method was found to range between 0.2 μm and 0.3 μm, as illustrated in the Figure 4.13. The external factors, along with the inherent surface variations of the substrate, and the limitations of the profiler could have influenced the measurement results, as discussed earlier.

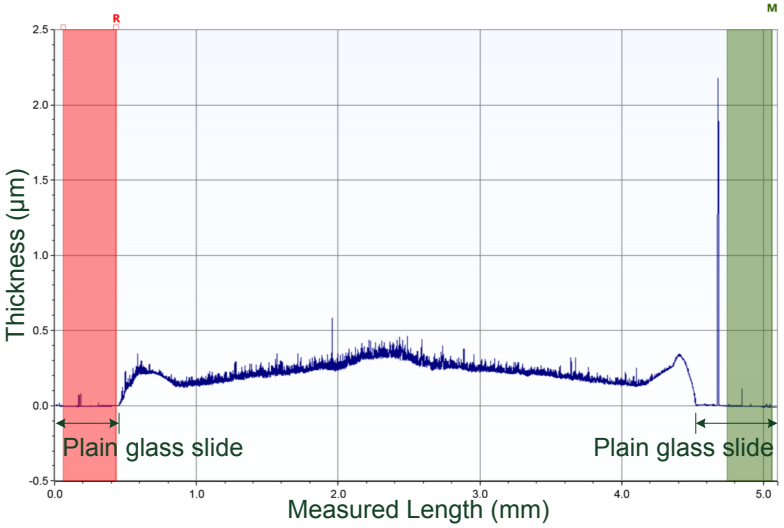

Figure 4.13: The thickness of the Matrigel^{TM} coating as obtained from the profilometer. About 0.2 mm from the start and the end of the trace is plain glass surface.

Thin Gel Method

The surface profile acquired a few hours after the coating, and along a secant line closer to the circumference of the coated surface is shown in the Figure 4.14. The thickness of the coating varied between 4.2 μm and 4.8 μm, as can be inferred from the figure below.

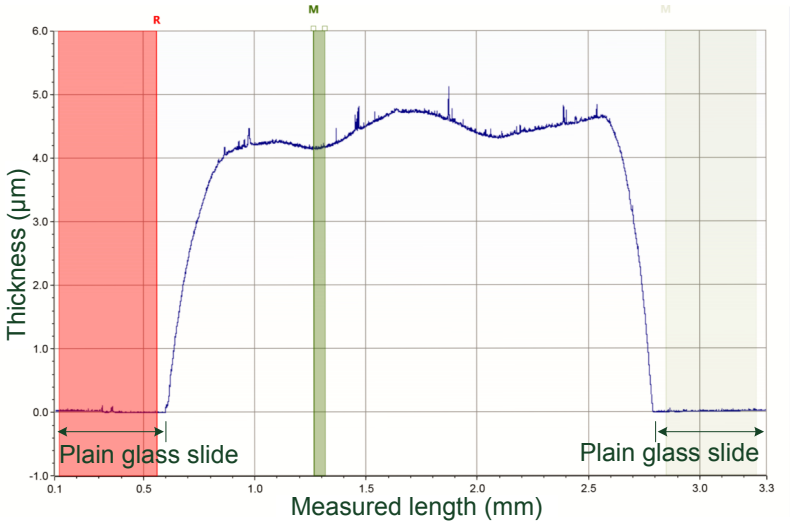

Figure 4.14: The thickness of the Matrigel^{TM} coating as obtained from the profilometer a few hours after the coating. About 0.5 mm from the start and the end of the trace is plain glass surface.

The subsequent measurement along the center of the coated surface was carried out 24 hours later, allowing enough time for the gel in the middle to dry. The surface variations observed are illustrated in Figure 4.15.

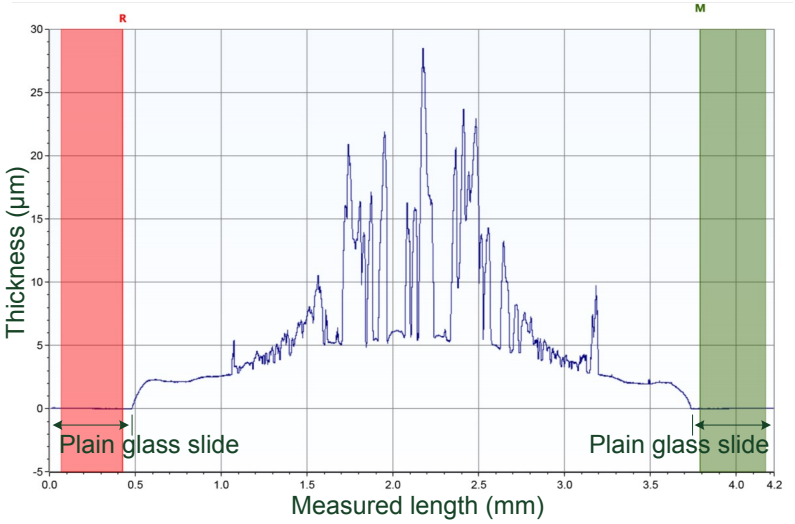

Figure 4.15: The surface trace of Matrigel^{TM}, obtained from the center of the coated surface, approximately 24 hours after the previous measurements. About 0.5 mm from the start and the end of the trace is plain glass surface.

The thickness of the coating was confined to about 2 μm or 3 μm along the periphery, as presented in Figure 4.15, but a steep rise was observed along the center of the coated surface. The deviations were bound between 5 μm and 28 μm, and the 'spikes' were corresponding to the solid patterns observed along the center of the gel, as pictured in Figure 4.16. Similar structures with variations in height ranging from 100 nm to over 300 nm were observed by Koivisto (2013) using AFM. The quantity and the concentration of Matrigel^{TM} however varies, along with the protocol followed for coating Matrigel^{TM}, which may explain the substantial difference between the two studies.

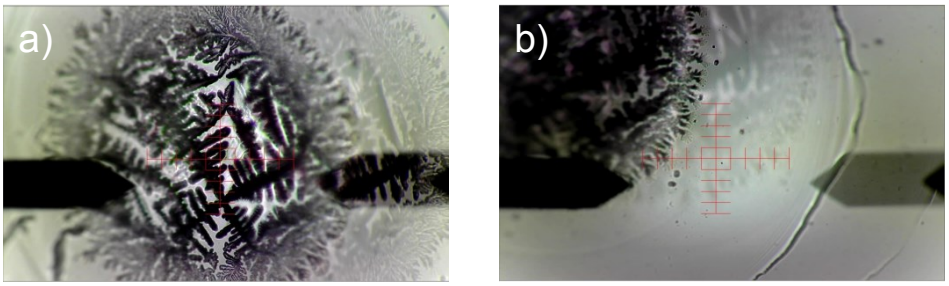

Figure 4.16: The solid patterns formed along the center of the gel is represented in (a), and the relatively clear gel along the periphery is imaged in (b).

During the process of coating, the dominant cohesive forces between the molecules of the Matrigel^{TM} matrix restricted it from spreading evenly over the substrate, and this convex shape was more or less retained as the matrix gelled, resulting in a substantial change in the thickness, as the measurement progressed from the periphery towards the centre of the coated surface. This phenomenon is noticeable from the images presented in the Figures A.1, and A.2 in the appendix.

Besides, as the gel dried, it shrunk in size and reduced to almost half the original thickness measured earlier. The measurements carried out about 24 hours later and along the perimeter of the gel in Figure 4.17, demonstrates this proposition of the thickness being halved from that obtained in Figure 4.14 earlier. Therefore, the thickness obtained along the center of the gel may not accurately represent the actual thickness of the gel formed on the surface originally.

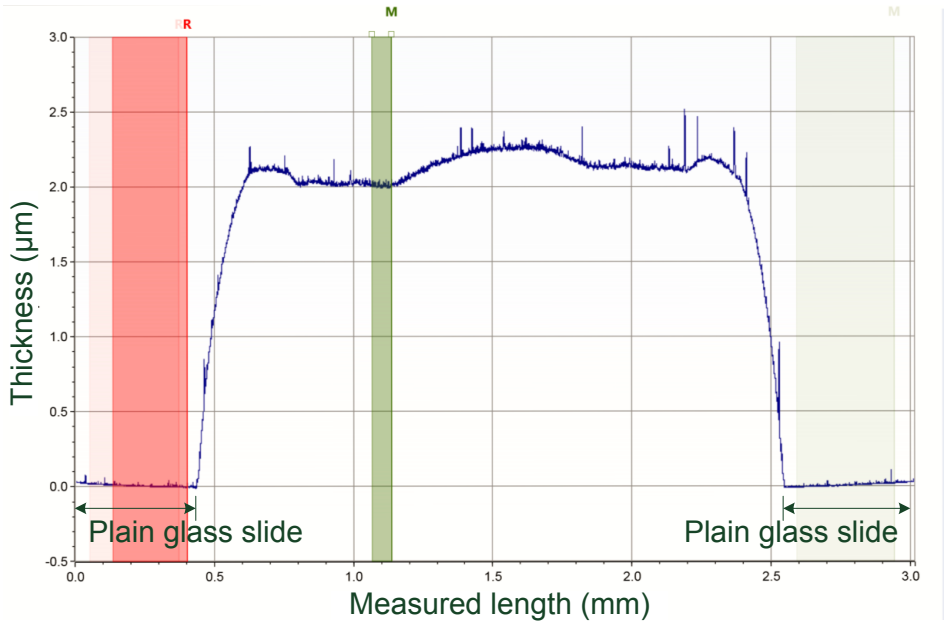

Figure 4.17: The surface trace of the Matrigel^{TM} coated surface, acquired along the periphery of the gel and about 24 hours from the initial measurements.

In fact, Matrigel^{TM} thickness measured in both the thin coating and the thin gel methods may not correspond to the actual thickness of the coating on the MEA surface, as unlike electrostatic self assembly, wherein a thin and a relatively uniform coating is expected, a change in the concentration of Matrigel^{TM} significantly affects the thickness of the coating. As extensive dilution of Matrigel^{TM} can even yield a thin, non-gelled protein layer. Without any structures to hold or limit the Matrigel^{TM} matrix on the substrate during coating, it spilled over to the surrounding area. This certainly would have affected the concentration of Matrigel^{TM} and by extension the thickness of the coating, possibly.

Furthermore, the change in the contact angle of the matrix, owing to the differences in the degree of wetting of the PDMS enclosed MEA surface and the uninterrupted expanse of the microscopic slide, could have had significant repercussions on the measurements.

4.4 Surface Roughness Measurements

The changes in the RMS value of surface roughness R_q of the silicon nitride surfaces and the reference electrode of the MEAs, with the addition of the PEI and laminin were studied using AFM, and the results of the experiment are presented in this section.

4.4.1 Surface Characterisation of the Silicon Nitride Surfaces

The surface roughness of the silicon nitride layer deposited over the glass surface and the titanium track of the MEA, was determined both before and after coating the MEAs with PEI and laminin as shown in figure 4.18(b). The respective changes in the surface area ratio, which is the increment of the measured surface area relative to the projected area in the XY plane, is plotted in Figure 4.18(a).

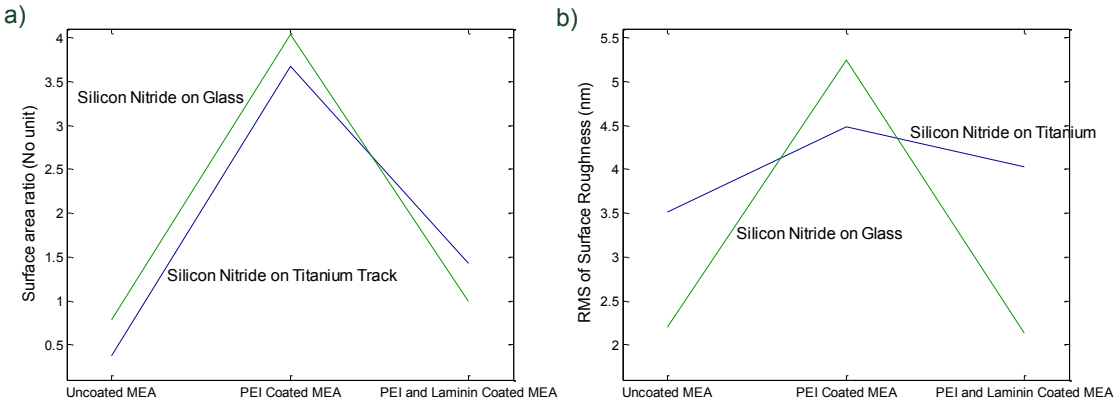

Figure 4.18: The change in the surface area ratio of the silicon nitride surfaces of the MEA, before and after coating is represented in (a), and the corresponding change in the RMS value of surface roughness is presented in (b).

The RMS value of surface roughness, and the surface area ratio of the silicon nitride layer increases with the addition of PEI, but however decreases with the addition of laminin. This implies that the addition of PEI results in an increase in the number of peaks, which are then smoothed by laminin. Three dimensional surface maps of the silicon nitride coated glass surface are rendered in the Figures 4.19, 4.20, and 4.21 to illustrate the same. The surface traces of the silicon nitride deposited titanium track is presented by the Figures B.1, B.2, and B.3 in the appendix.

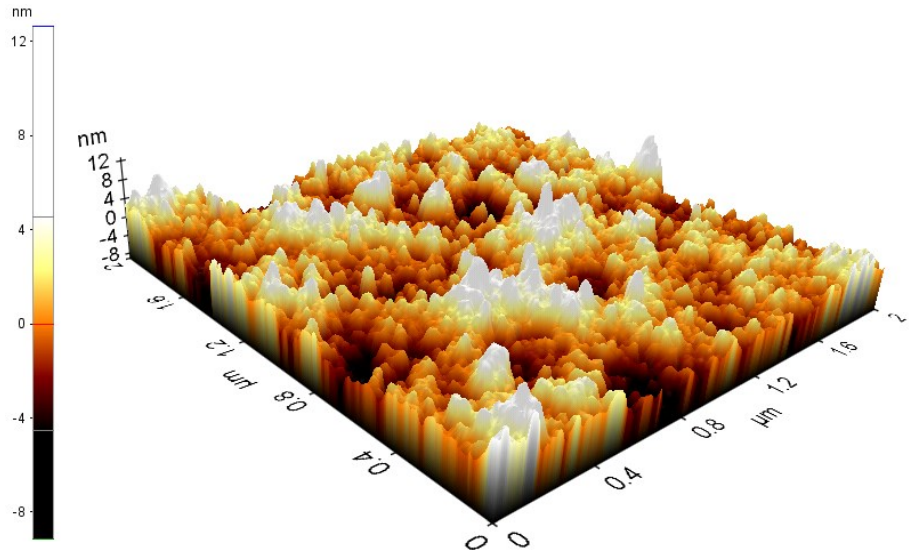

Figure 4.19: The three dimensional surface map, over a 2 µm × 2 µm silicon nitride covered glass surface of the uncoated MEA, as obtained from AFM.

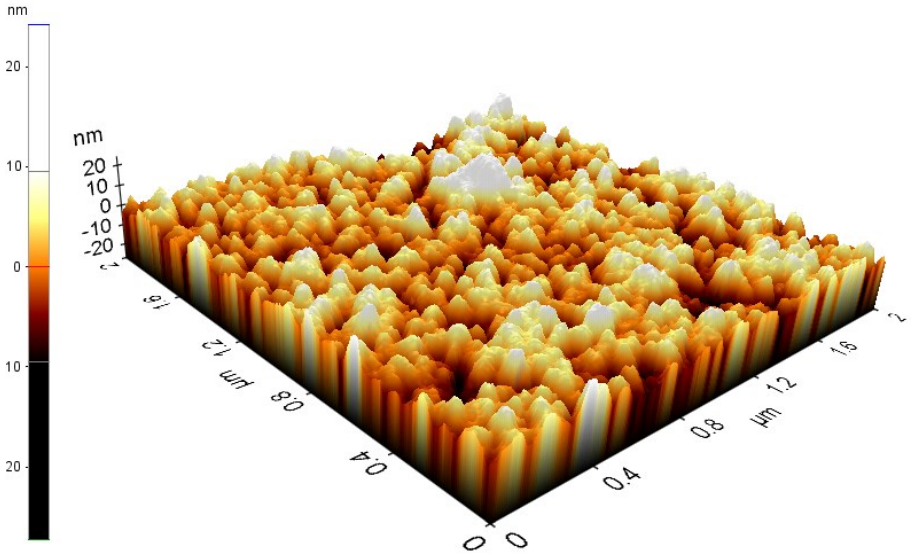

Figure 4.20: A three dimensional surface map as acquired using AFM, over a 2 µm × 2 µm silicon nitride covered glass surface of the MEA coated with PEI.

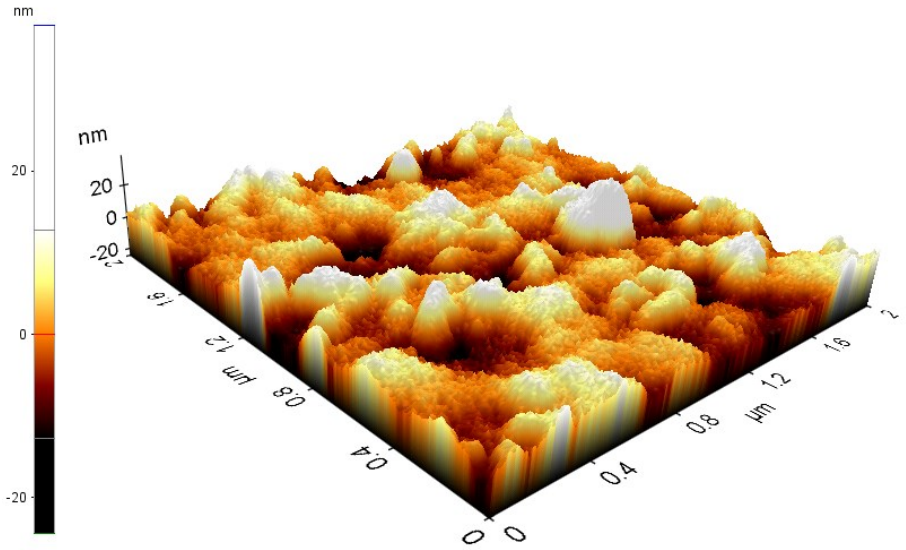

Figure 4.21: The three dimensional surface map, over a 2 µm × 2 µm silicon nitride covered glass surface of the MEA coated with PEI and laminin.

4.4.2 Surface Characterisation of the Reference Electrode

Similar to the surface characterisation of the silicon nitride surface, the surface area ratio, and the surface roughness of the reference electrode is determined as in Figure 4.22. On addition of PEI, the spikes of the highly uneven reference electrode appear to shrivel as represented by the decrease in the surface area ratio. However this decline does not level the surface much, rather it increases the overall surface roughness by a few nanometres. Further, with the addition of laminin, both the surface area ratio and the surface roughness rise, indicating an escalation in the unevenness.

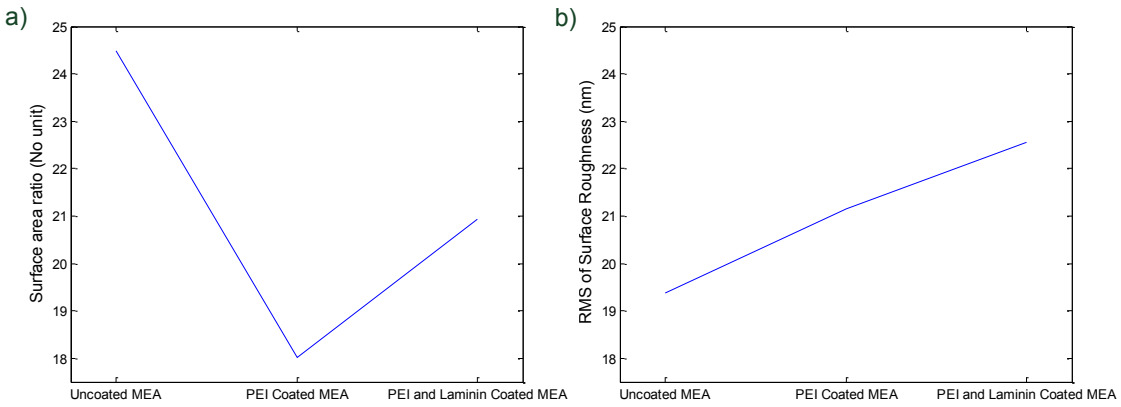

Figure 4.22: The change in the surface area ratio of the reference electrode of the MEA, before and after coating is represented in (a), and the corresponding change in the surface roughness is presented in (b).

The three dimensional surface maps of the reference electrode, captured with the AFM, before and after coating are shown in Figures 4.23, 4.24, and 4.25 below.

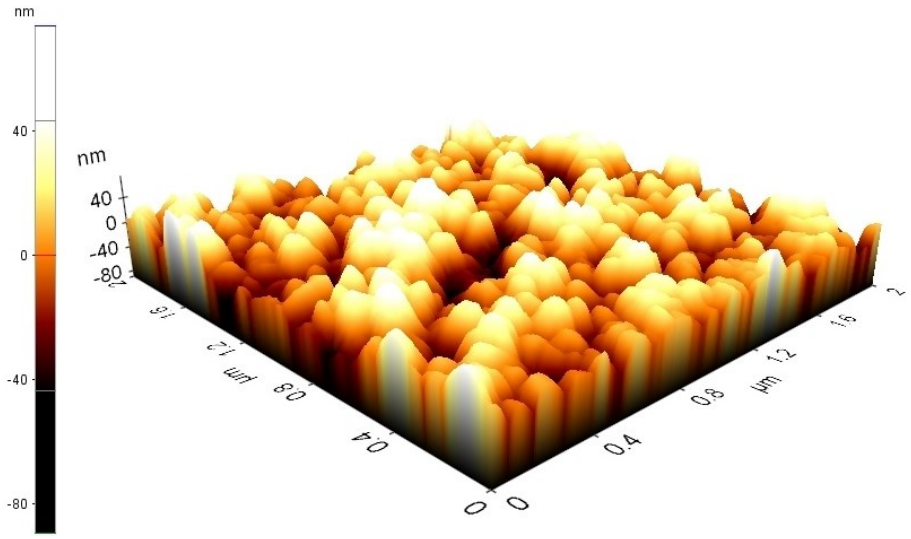

Figure 4.23: The three dimensional surface map obtained with AFM, over a 2 µm × 2 µm reference electrode surface of the uncoated MEA.

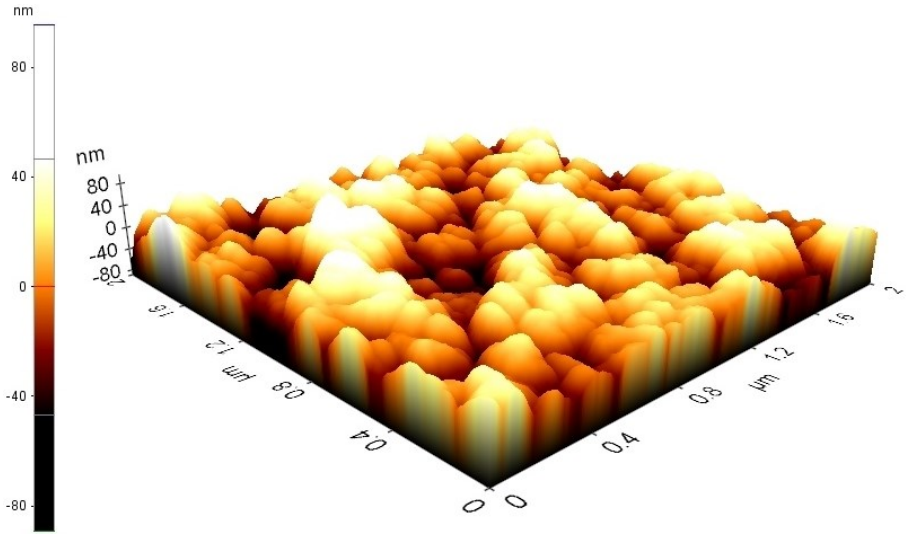

Figure 4.24: A three dimensional surface map as acquired using AFM, over a 2 µm × 2 µm reference electrode surface of the MEA coated with PEI.

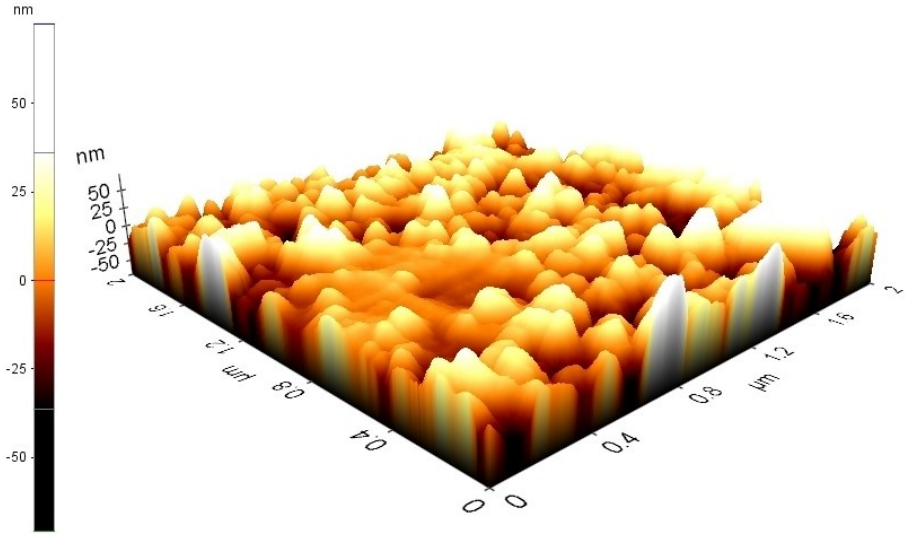

Figure 4.25: The three dimensional surface map, over a 2 μm × 2 μm surface of the reference electrode of the MEA coated with PEI and laminin.

A major shortcoming of these measurements however, is that surface characterisation was performed on not one, but three different MEAs, one each for the uncoated and the two other coated measurements. Therefore, the inherent differences in the surface roughness of the MEAs could have affected the measurement results. Also the MEA used for the coating of PEI had been in general use for a relatively longer interval than the other two MEAs, and hence chances are that it could have undergone surface modifications, over prolonged exposure to the cell and the culture medium. Besides, no previous results could be procured, for direct comparison of the results.

4.5 Adsorption Measurements

The differential molecular adsorption with varying concentrations of laminin was studied along with the kinetics, using surface plasmon resonance technique, and the outcomes of these studies are detailed in this section.

Differential Adsorption of Laminin

The changes in the SPR angle with the adsorption of 0.05 % (w/v) PEI, 20 μg/ml and 40 μg/ml of laminin, for the wavelengths of 670 nm and 785 nm are obtained as in the Figure 4.26. Although not radical, a significant change in the SPR angle can be observed between the concentrations of laminin, denoting the differential adsorption of laminin to the sensor slide. But this change may not exactly correspond to the binding of laminin with PEI, as will be discovered in the subsequent measurements. The variations in the width and the depth of the resonance curves are a result of

the differential optical adsorption within the metal and the radiation losses owing to the surface roughness.

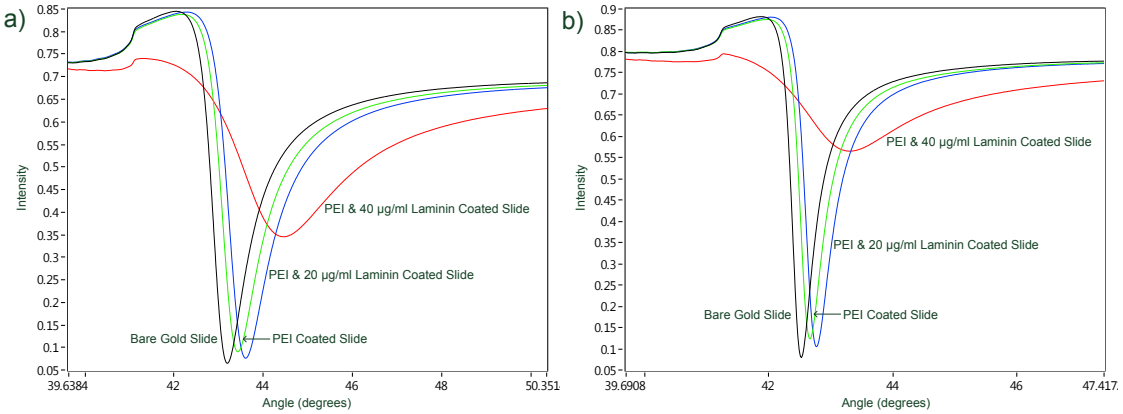

Figure 4.26: The changes in the SPR angle with the addition of PEI, 20 µg/ml and 40 µg/ml of laminin for the wavelengths of 670 nm are presented in (a), and the changes corresponding to the wavelength of 785 nm are plotted in (b).

With a further increase in the laminin concentrations to 80 μg/ml, the changes observed in the SPR angles are recorded in Figure 4.27. No difference in the SPR angle was observed with the addition of PEI, which signifies that PEI molecules had not adsorbed to the sensor slide. This could be attributed to the mishap during coating, that caused PEI to settle down at the bottom of the container. However as the experiment progressed thereafter with the addition of laminin, the SPR angle changed significantly, suggesting that laminin might have randomly adsorbed to the gold surface directly, rather than interacting with the PEI molecule as intended originally. A summary of the results for PEI and varying laminin concentrations is provided in Table 4.5.

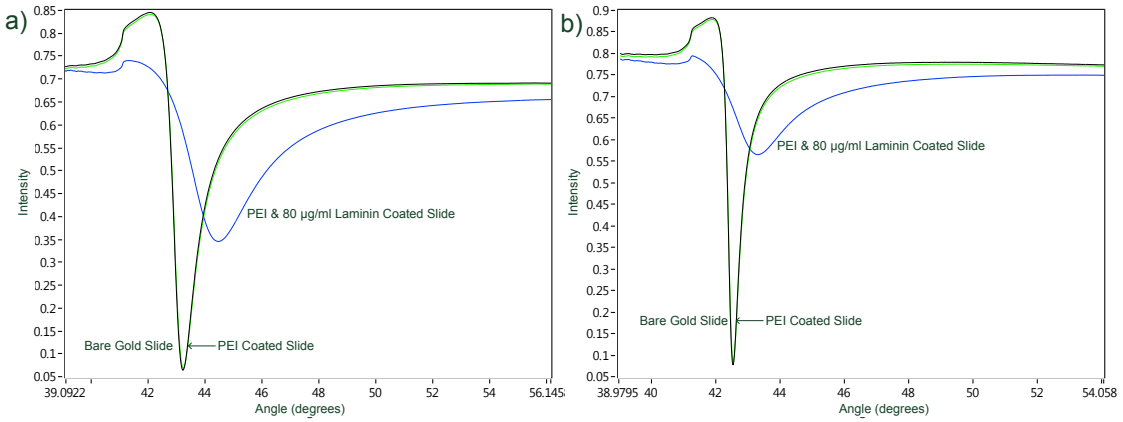

Figure 4.27: The changes in the SPR angle with the addition of PEI, 80 µg/ml of laminin for the wavelengths of 670 nm are presented in (a), and the corresponding changes for the wavelength of 785 nm are rendered in (b).

Table 4.5: The changes in the SPR angle with the adsorption of PEI, 20 μg/ml, 40 μg/, and 80 μg/ml of laminin.

Concentration of Laminin (μg/ml)	SPR Angle (degree)		
	Bare Gold	0.05 % PEI Coated Surface	PEI & Laminin Coated Surface
Laser Wavelength: 670 nm			
20	43.20	43.38	43.54
40	43.20	43.50	44.10
80	43.21	43.23	44.46
Laser Wavelength: 785 nm			
20	42.52	42.64	42.74
40	43.53	42.69	43.08
80	42.53	42.54	43.31

Kinetics Study

The sensor slides were exposed initially to PEI and to laminin subsequently, and the rate of adsorption of the molecules to the slide over time was studied, as a function of the change in the SPR angle. The observed changes in the SPR angle are provided in the Figure 4.28 below.

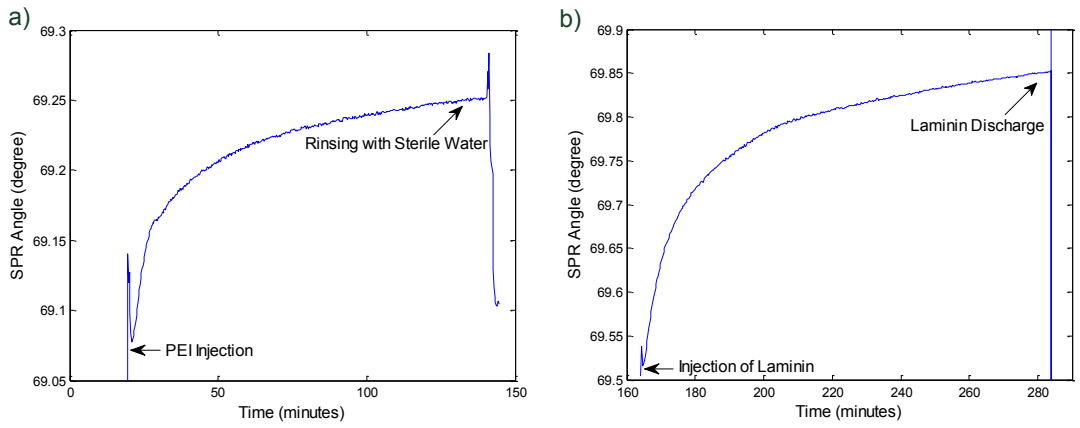

Figure 4.28: The changes in the SPR angle observed over time with the adsorption of PEI are presented in (a), and the respective changes with the adsorption of laminin are represented in (b).

Although most of the binding happens during the first 60 minutes after the injection of PEI, the curve does not flatten out before PEI is rinsed with sterile water. A similar trend is observed with laminin, suggestive of adsorption occurring until the very end. The overshoots during injection and the ejection of the fluids

are probably due to the changes in the flow, and may partly be due to differences in the temperature. Although the solutions were warmed to a temperature of 37 °C in an incubator prior to injection, losses are bound to happen while handling them at room temperature.

The SPR angles in Figure 4.28 may not correspond with those obtained from the adsorption measurements. This staunch divergence of the SPR angle(s) from the previous study is due to the differences in the refractive index of the media adjoining the sensor slide. While the adsorption measurements were carried out in air or a low refractive index media, kinetics study was performed in the presence of PEI and laminin solutions having relatively higher refractive indices.

However, measurements were made in air medium subsequently as presented in Figure 4.29, where the SPR angles are in line with the earlier findings. The SPR angles measured in air medium after the discharge of PEI, and Laminin exhibit a relative increase when compared against that of the bare gold surface, and the PEI coated surface respectively, which represent the adsorption of the corresponding molecules to the surface of the sensor slide.

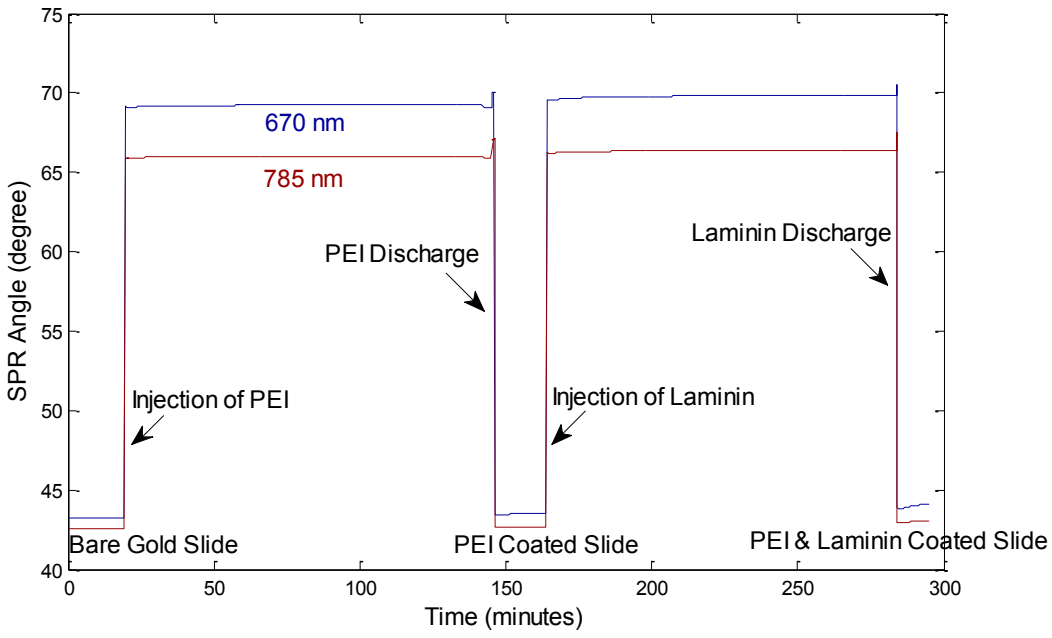

Figure 4.29: The kinetics study to observe the change in the SPR angle over time with the adsorption of PEI and laminin.

5. CONCLUSIONS

The aim of the study was to evaluate the effect of the coatings on the overall performance of the MEAs. In addition, an attempt was also made to study the thickness, and the surface variations of the MEA coatings.

Three different coatings polyethyleneimine and laminin, gelatin, and Matrigel^{TM} were studied, and their influence on the impedance and the noise characteristics of the MEA was evaluated. Commercial 6 well MEAs were used alongside the Standard 8 $\times$ 8 MEA for the measurements. The MEAs were coated with the surface molecules, and the differences in the impedance magnitudes, and the RMS noise voltages upon coating were analysed. Custom made PDMS structures were used to limit the coating material over the MEA surface. PEI and laminin, and gelatin did not facilitate any significant difference in the electrode impedance or the noise. Besides employing Matrigel^{TM} as such, it was diluted to one tenth of its concentration, and the differences arising with the dilution were studied. Impedance changes in both these cases were substantial, with Matrigel^{TM} in its original concentration effecting the most change. However, irrespective of the concentration, Matrigel^{TM} brought about a very modest increase in the RMS noise amplitude of the electrodes.

In order to realise the repercussions in real life situations, experiments were conducted with the neural cells. The changes in the electrode impedances and the noise were recorded, but due to limitations in imaging the cells plated on top of the MEAs, no conclusions could be made. The opaque titanium nitride electrodes obscured the field of view when pictured from the bottom, and neither the position nor the orientation of the cell(s) atop the electrode surface could be ascertained.

The thickness of the nano-scale PEI and laminin, and gelatin coatings could not be reliably measured using the stylus profilometer, as the inherent surface variations of the substrate affected the measurements. The thickness of the Matrigel^{TM} coating on the other hand was sizeable to overcome these variations, and following in line with the literature studies increased with the concentration. The coating was formed over the uninterrupted expanse of a microscopic slide, and differences in the degree of wetting, and spillage could have impacted the results.

Surface characterisation of the MEA surface, coated with PEI and laminin was carried out using the AFM. The silicon nitride surface, which is relatively uniform compared to the reference electrode, displayed an increase in roughness with the

addition of PEI, which then subdued with the exposure to laminin. The uneven reference electrode on the other hand exhibited an increased surface roughness with the addition of both PEI and laminin. However, it is to be noted that the measurements were made on not one, but three different MEAs, and the intrinsic variations in the surface roughness of the MEAs could have manipulated the outcome of the experiment.

The differential adsorption of laminin with the concentration was estimated using SPR, as a change in the SPR angle. Laminin was found to randomly adsorb to the gold sensor slide rather than bind with PEI as intended. Also, kinetics study suggests the molecular adsorption of both PEI and laminin to have taken place until their very removal after two hours.

Further study in this regard is required, and the shortcomings of this thesis have to be resolved, in order to obtain conclusive results. First of all, the cells need to be imaged from top, and at a higher resolution if the changes in impedance are to be related to the positioning of the cell(s). Micro channels, or other suitable alternatives need to be devised for thickness measurements, so as to restrict the coated area and to overcome the limitations endured due to the surface variations of the substrate. Finally, surface texture analysis is to be performed with the same reference surface in order to minimize uncertainties.

REFERENCES

Abate, A., Lee, D., Do, T., Holtze, C. & Weitz, D. 2008. Glass coating for PDMS microfluidic channels by sol-gel methods. Lab Chip, 8, pp. 516-518.

Ahmadi, M.M. & Jullien, G.A. 2009. Current-Mirror-Based Potentiostats for Three-Electrode Amperometric Electrochemical Sensors. IEEE Transactions on Circuits and Systems - I 56, 7, pp. 1339-1348.

Aumailley, M., Bruckner-Tunderman, L., Carter, W.G., Deutzmann, R., Edgar, D., Ekblom, P., *et al.* 2005. A simplified laminin nomenclature. Matrix Biology, 24, 5. pp. 326-332.

Aurien-Blajeni, B., Beebe, X., Rauh, R.D. & Rose, T.L. 1989. Impedance of hydrated iridium oxide electrodes. Electrochimica Acta 34, pp. 795-802.

Bal-Price, A.K., Hogberg, H.T., Buzanska, L., Lenas, P., Vliet, E.V. & Hartung, T. 2010. In vitro developmental neurotoxicity (DNT) testing Relevant models and endpoints. NeuroToxicology, 31, pp. 545-554.

Bhushan, B. 2013. Principles and Applications to Tribology. Second edition. New York, USA, John Wiley & Sons, Ltd. 980 p.

Bhushan, B. 2008. Nanotribology, Nanomechanics and Material Characterization. In: Bhushan, B. (ed.). Nanotribology and Nanomechanics: An Introduction. Second edition. Heidelberg, Germany, Springer-Verlag Berlin Heidelberg. pp. 311-416.

Bockris, J.O'M., Reddy, A.K.N. & Maria, G.A. 2002. Modern Electrochemistry 2A: Fundamentals of Electrodics. Second edition. New York, USA, Kluwer Academic Publishers. 1534 p.

Borkholder, D., A. 1998. Cell based biosensors using microelectrodes. Dissertation. Stanford. Stanford University. Department of Electrical Engineering. 229 p.

Bougas, K., Stenport, V.F., Tengvall, P., Currie, F. & Wennerberg, A. 2011. Laminin Coating Promotes Calcium Phosphate Precipitation on Titanium Discs in vitro. Journal of Oral and Maxillofacial Research 2(4), 5.

Boxshall, K., Wu, M.H., Cui, Z., Watts, J.F. & Baker, M.A. 2006. Simple surface treatments to modify protein adsorption and cell attachment properties within a poly(dimethylsiloxane) micro-Bioreactor. Surface and Interface Analysis, 38, pp. 198-201.

Chi, T., Ballinger, T., Olds, R. & Zecchino, M. 2010. Surface texture Analysis Using Dektak Stylus Profilers. Application note. Bruker Corporation. 4 p.

Cogan, S.F. 2008. Neural stimulation and recording electrodes. Annual Review of Biomedical Engineering 10. pp. 275-309.

Dektak XT Stylus Profiling System - Brochure. 2011. Bruker Nano Surfaces Division, USA. Bruker Corporation. 8 p.

Dektak XT Stylus Profiler - User Manual. 2011. Bruker Nano Surfaces Division, USA. Bruker Corporation. 83 p.

Egert, U. & Meyer, T. 2005. Heart on a Chip – Extracellular Multielectrode Recordings from Cardiac Myocytes in Vitro. In: Dhein, S., Mohr, F.W. & Delmar, M. (ed.). Practical Methods in Cardiovascular Research. Heidelberg, Germany, Springer-Verlag GmbH & Co. pp. 43-453.

Fejtl, M., Stett, A., Nisch, W., Boven, K.H. & Möller, A. 2006. On MicroElectrode Array Revival: Its development, Sophistication of Recording, and Stimulation. In: Taketani, M. & Baudry, M. (ed.). Advances in Network Electrophysiology: Using MultiElectrode Arrays. New York, USA, Springer Science + Business Media, Inc. pp. 24-37.

Franks, W., Schenker, I., Schmutz, P. & Hierlemann, A. 2005. Impedance Characterization and Modeling of Electrodes for Biomedical Applications. IEEE Transactions on Biomedical Engineering 52, 7, pp. 1295-1302.

Gesteland, R.C., Howland, B., Lettvin, J.Y. & Pitts, W.H. 1856. Comments on Microelectrodes. Proceedings of the IRE, November 1856, pp. 1856-1862.

Grumet, A.E., Wyatt J.L. & Rizzio, J.F. 2000. Multi-electrode stimulation and recording in the isolated retina. Journal of Neuroscience Methods 101, 1, pp. 3-42.

Gross, G.W. 1979. Simultaneous Single Unit Recording in vitro with a Photoetched Laser Deinsulated Gold Multimicroelectrode Surface. IEEE Transactions on Biomedical Engineering, BME-26, 5, pp. 273-279.

Guo, J., Yuan, J. & Chan, M. 2012. Modeling of the Cell-Electrode Interface Noise for Microelectrode Arrays. IEEE Transactions on Biomedical Circuits and Systems 6, 6, pp. 605-613.

Hafizovic, S., Heer, F., Ugniwenko, T., Frey, U., Blau, A., Ziegler, C. & Hierlemann, A. 2007. A CMOS-based microelectrode array for interaction with neuronal cultures. Journal of Neuroscience Methods 164, 1, pp. 9-106.

He, W. & Bellamkonda, R.V. 2004. Nanoscale neuro-integrative coatings for neural implants. Biomaterials 26, (2005), pp. 2983-2990.

Heer, F., Hafizovic, S., Ugniwenko, T., Frey, U., Roscic, B., Blau, A. & Hierlemann, A. 2007. Using microelectronics technology to communicate with living cells. 29th Annual International Conference of the IEEE EMBS, Cité Internationale, Lyon, France, August 22-26, 2007. pp. 608-6084.

Hemmilä, S., Cauich-Rodríguez, J.V., Kreutzer, J. & Kallio, P. 2012. Rapid, simple, and cost-effective treatments to achieve long-term hydrophilic PDMS surfaces. Applied Surface Science, 258, 24, pp. 9864-9875.

Homola, J., Yee, S.S. & Gauglitz, G. 1999. Surface plasmon resonance sensors: review. Sensors and Actuators B: Chemical, 54, 1-2, pp. 3-15.

Impedance Testing Device, MEA-IT Manual. 2012. Reutlingen, Germany. Multi Channel Systems MCS GmbH. 26 p.

Ingrid, A.M.R., Damen, C.A., van der Schaft, D.W.J., Groenewegen, G. & Griffioen, A.W. 1998. Effect of culture conditions on endothelial cell growth and responsiveness. Tissue & Cell, 30, 5. pp. 525-530.

IviumSoft User Manual. 2010. Ivium Technologies, Eindhoven, Netherlands. User Manual. 143 p.

Johnstone, A.F.M., Gross, G.W., Weiss, D.G., Schroeder, O.H.U., Gramowski, A. & Shafer, T.J. 2010. Microelectrode arrays A physiologically based neurotoxicity testing platform for the 21st century. NeuroToxicology, 31, pp. 331-350.

Jones, I.L., Livi, P., Lewandowska, M.K., Fiscella, M., Roscic, B. & Hierlemann, A. 2011. The potential of microelectrode arrays and microelectronics for biomedical research and diagnostics. Analytical and Bioanalytical Chemistry 399, 7, pp. 231-2329.

Joye, N., Schmid, A. & Leblebici, Y. 2009. Electrical modeling of the cell-electrode interface for recording neural activity from high-density microelectrode arrays. Neurocomputing 73, pp. 250-259.

Karp, F.B., Bernotski, N.A., Valdes, T.I., Bohringer, K.F. & Ratner, B.D. 2008. Foreign body response investigated with an implanted biosensor by in situ electrochemical impedance spectroscopy. IEEE Sensors Journal 8, pp. 104-112.

Kehat, I., Gepstein, A., Spira, A., Itskovitz-Eldor, J. & Gepstein, L. 2002. High-Resolution Electrophysiological Assessment of Human Embryonic Stem Cell-Derived Cardiomyocytes A Novel In Vitro Model for the Study of Conduction. Circulation Research, 91, pp. 659-661.

Kleinman, H.K. & Martin, G.R. 2005. Matrigel: Basement membrane matrix with biological activity. Seminars in Cancer Biology 15, pp. 378-386.

Kleinman, H.K., McGarvey, M.L., Hassell, J.R., Star, V.L., Cannon, F.B., Laurie, G.W., & Martin, G.R. 1985. Basement Membrane Complexes with Biological Activity. Biochemistry (2016), 25. pp. 312-318.

Koivisto, J. 2013. Differentiation of human induced pluripotent stem cells into peripheral neural cells. Master of Science Thesis, Tampere. Tampere University of Technology. 96 p.

Kremer, F. & Schönhals, A. 2003. Broadband Dielectric Measurement Techniques. In: Kremer, F., Schönhals, A. (ed). Broadband Dielectric Spectroscopy. Heidelberg, Germany, Springer-Verlag Berlin Heidelberg. pp. 35-56.

Kreutzer, J., Lappalainen, R., Ylä-Outinen, L., Narkilahti, S., Mikkonen, J. & Kallio, P. 2009. Laminin coated PDMS surfaces for long-term MEA measurements of hESC-derived neural networks. Proceedings of the Symposium on Microelectrode Arrays in Tissue Engineering, pp. 23-25.

Lakard, S., Herlem, G., Propper, A., Kastner, A., Michel, G., Vallès-Villarreal, Gharbi, T. & Fahys, B. 2004. Adhesion and proliferation of cells on new polymers modified biomaterials. Bioelectrochemistry 62, pp. 19-27.

Lee, J.N., Park, C. & Whitesides, G. 2003. Solvent compatibility of poly(dimethylsiloxane)-based microfluidic devices. Analytical Chemistry, 75, pp. 6544-6554.

Lindsay, R.M., Evison, C.J. & Winter, J. 1991. Culture of adult mammalian peripheral neurons. In: Chad, J. & Wheal, H. (ed).Cellular Neurobiology: A Practical Approach. New York, USA, Oxford University Press. pp. 3-17.

Liu, B.F., Ma, J., Xu, Q.Y. & Cui, F.Z. 2006. Regulation of charged groups and laminin patterns for selective neuronal adhesion. Colloids and Surfaces B: Biointerfaces 53, pp. 175-178.

Liu, J.J., Li, H., Zhang, F., Li, X., Wang, L. & Chen, Y. 2010. Online impedance monitoring of yeast cell culture. Microelectronic Engineering 88, (2011). pp. 1711-1713.

Ludwig, K.A., Uram, J.D., Yang, J., Martin, D.C. & Kipke, D.R. 2006. Chronic neural recordings using silicon microelectrode arrays electrochemically deposited with a poly(3,4-ethylenedioxythiophene) (PEDOT) film. Journal of Neural Engineering 3, pp. 59-70.

Macdonald, J.R. & Johnson, W.B. 2005. Fundamentals of Impedance Spectroscopy. In: Barsoukov, E. & Macdonald, J.R. (ed.). Impedance Spectroscopy: Theory, Experiment, and Applications. Second edition. New Jersey, USA, John Wiley & Sons, Inc. 595 p.

Mata, A., Fleischman, A.J. & Roy, S. 2005. Characterization of polydimethylsiloxane (PDMS) properties for biomedical micro/nanosystems. Biomedical Microdevices, 7, pp. 281-293.

Matrigel™: Guidelines for use. 2012. BD Biosciences - Discovery Labware. 4 p.

McCrackin, F.L. 1969. A Fortran Program for Analysis of Ellipsometer Measurements. Technical Note. Washington, D.C., USA, U.S. Government Printing Office. 79 p.

McDonald. J.C., Duffy, D.C., Anderson, J.R., Chiu, D.T., Wu, H., Schueller, O.J. & Whitesides, G.M. 2000. Fabrication of microfluidic systems in poly(dimethylsiloxane). Electrophoresis, 21, pp. 27-40.

MEA2100-System Manual. 2013. Reutlingen, Germany. Multi Channel Systems MCS GmbH. 66 p.

Merkel, T.C., bondar, V.I., Nagai, K., Freeman, B.D. & Pinnau, I. 2000. Gas sorption, diffusion, and permeation in poly(dimethylsiloxane). Journal of Polymer Science, Part B: Polymer Physics, 38, pp. 415-434.

Microelectrode Array (MEA) Manual. 2012. Reutlingen, Germany. Multi Channel Systems MCS GmbH. 116 p.

Monahan, J., Gewirth, A., Nuzzo, R. 2002. Indirect fluorescence detection of simple sugars via high-pH electrophoresis in poly(dimethylsiloxane) microfluidic chips. Electrophoresis, 23, pp. 2347-2354.

Montenegro, M.I., Queirós, M.A. & Daschbach, J.L.(ed.). 1991. Microelectrodes: Theory and Applications. Dordrecht, Netherlands, Kluwer Academic Publishers Group. 501 p.

Niklasson, G.A., Johsson, A.K. & Strømme, M. 2005. Impedance Response of Electrochromic Materials and Devices. In: Barsoukov, E. & Macdonald, J.R. (ed.). Impedance Spectroscopy: Theory, Experiment, and Applications. Second edition. New Jersey, USA, John Wiley & Sons, Inc. 595 p.

Non-Contact Mode AFM vs. Tapping Mode AFM. 2013. Korea. Park Systems Corp., Unpublished report. 3 p.

Product Information: Gelatin. 2013. Sigma-Aldrich Co. LLC. 3 p.

Product Information: LIVE/DEAD® Viability/Cytotoxicity Kit. 2005. Molecular Probes Inc. 7 p.

Product Information: Poly(ethyleneimine) solution. 2011. Sigma-Aldrich Co. LLC. 1 p.

Randles, J.E.B. 1947. Kinetics of rapid electrode reactions. Discussions of the Faraday Society, 1, pp. 11-19.

Reppel, M., Pillekamp, F., Lu, Z.J., Halbach, M., Brockmeter, K., Fleischmann, B.K. & Hescheler, J. Microelectrode Arrays A New Tool to Measure Embryonic Heart Activity. Journal of Electrocardiology, 37, pp. 104-109.

Sauerbrey, G. 1959. Verwendung von Schwingquarzen zur Wägung dünner Schichten und zur Mikrowägung. Zeitschrift für Physik, 155, 2, pp. 206-222.

Schirmeisen, A., Anczykowski, B., Hölscher, H. & Fuchs, H. 2008. Dynamic Modes of Atomic Force Microscopy. In: Bhushan, B. (ed.). Nanotribology and Nanomechanics: An Introduction. Second edition. Heidelberg, Germany, Springer-Verlag Berlin Heidelberg. pp. 235-277.

Shih, T.K., Chen, C.F., Ho, J.R. & Chuang, F.T. 2006. Fabrication of PDMS (polydimethylsiloxane) microlens and diffuser using replica molding. Microelectronic Engineering, 83, pp. 2499-2503.

SPR-Navi 210A User Manual. 2012. Version 1.0. BioNavis Oy Ltd., Tampere, Finland. User Manual. 28 p.

SPR-Navi Software Manual. 2012. Version 5.0. BioNavis Oy Ltd., Tampere, Finland. Software Manual. 27 p.

Thomas, Jr.C.A., Springer, P.A., Loeb, G.E., Berwald-Netter, Y. & Okun, L.M. 1972. A miniature microelectrode array to monitor the bioelectric activity of cultured cells. Experimental Cell Research, 74, 1, pp. 61-66.

True Non-Contact Mode™. 2013. Korea. Park Systems Corp., Unpublished report. 2 p.

Vancha, A.R., Govindaraju, S., Parsa K.V.L., Jasti, M., González-García M. & Ballestero, R.P. 2004. Use of polyethyleneimine polymer in cell culture as attachment factor and lipofection enhancer. BioMed Central Biotechnology 23, 4.

Wagennar, D.A., Madhavan, R., Pine, J. & Potter, S.M. 2005. Controlling Bursting in Cortical Cultures with Closed-Loop Multi-Electrode Stimulation. The Journal of Neuroscience 25, 3, pp. 68-688.

Wang, L., Sun, B., Ziemer, K.S., Barabino, G.A. & Carrier, R.L. 2010. Chemical and physical modifications to poly(dimethylsiloxane) surfaces affect adhesion of Caco-2 cells. Journal of Biomedical Materials Research Part A, 93, pp. 1260-1271.

Warburg, E. 1899. Über das Verhalten sorgenannter unpolarisbarer Electroden gegen Wechselstrom. Annalen der Physik und Chemie 67. pp. 493-499.

Ward, M.P., Rajdev, P., Ellison, C. & Irazoqui, P.P. 2009. Toward a comparison of microelectrodes for acute and chronic recordings. Brain Research 1282, pp. 183-200.

Weiland, J.D. & Anderson D.J. 2000. Chronic Neural Stimulation with Thin-Film, Iridium Oxide Electrodes. IEEE Transactions on Biomedical Engineering 47, 7, pp. 911-918.

Weiland, J.D., Anderson, D.J. & Humayun, M.S. 2002. In Vitro Electrical Properties for Iridium Oxide Versus Titanium Nitride Stimulating Electrodes. IEEE Transactions on Biomedical Engineering 49, 12, pp. 1574-1579.

Wong, I. & Ho, C.M. 2009. Surface molecular property modifications for poly(dimethylsiloxane) (PDMS) based microfluidic devices. Microfluidics and Nanofluidics, 7, pp. 291-306.

XE-100: High Accuracy Small Sample SPM. 2002. USA. Park Systems Corp., Originally PSIA Corp., User's Manual. 86 p.

XEI: Powerful Image Processing Tool for SPM Data. 2008. USA. Park Systems Corp., Software Manual. 177 p.

Xia, Y. & Whitesides, G.M. 1998. Soft Lithography. Angewandte Chemie International Edition, 37, 5, pp. 550-575.

Yang, H. & Wang, Y. 2009. Effects of concentration on nanostructural images and physical properties of gelatin from channel catfish skins. Food Hydrocolloids 23, 3. pp. 577-584.

Ylä-Outinen, L., Heikkilä, J., Skottman, H., Suuronen, R., Äänismaa, R. & Narkilahti, S. 2010. Human cell-based micro electrode array platform for studying neurotoxicity. Frontiers in Neuroengineering, 3, 111, pp. 1-9.

A. APPENDIX: THICKNESS MEASUREMENTS

The variations in the thickness of the Matrigel^{TM} coating as the measurement progressed from the periphery towards the center of the coated surface are represented in the Figures A.1, and A.2.

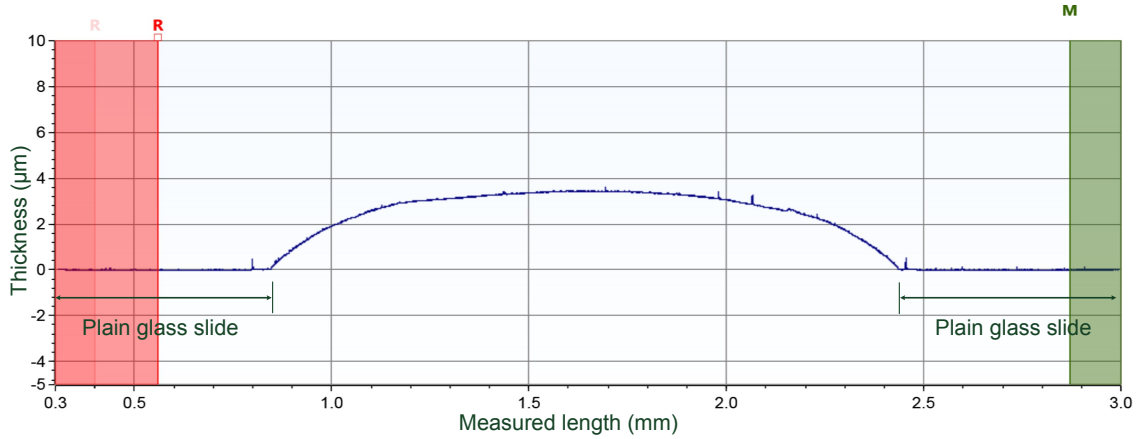

Figure A.1: The thickness of the Matrigel^{TM} coating as acquired from the periphery of the coated surface. About 0.5 mm from the start and the end of the trace is plain glass surface.

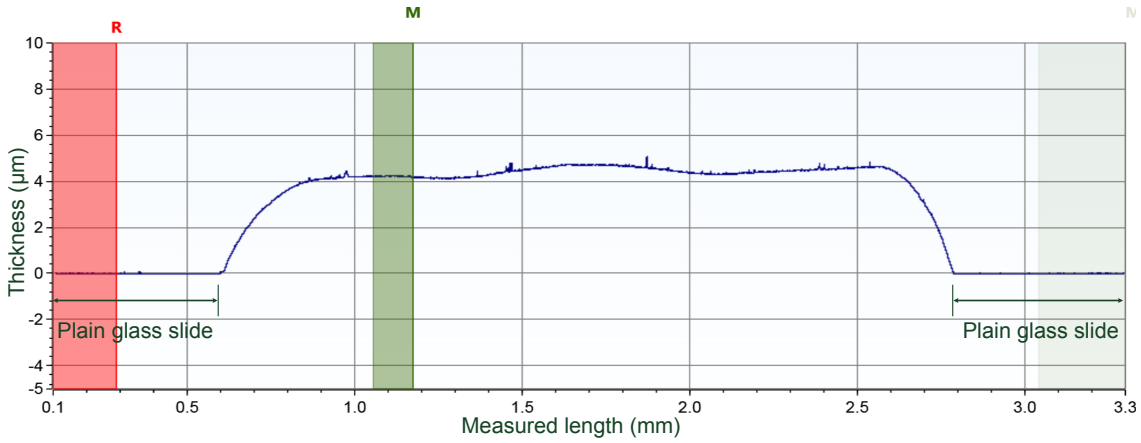

Figure A.2: The surface trace of the Matrigel^{TM} coating obtained a few millimetres away from the circumference, and towards the center of the coating. Approximately 0.5 mm from the start and the end of the trace is plain glass surface.

B. APPENDIX: SURFACE ROUGHNESS MEASUREMENTS

The three dimensional surface maps of the silicon nitride covered titanium track of the MEA, captured with the AFM before and after coating, are shown in Figures B.1, B.2, and B.3 below.

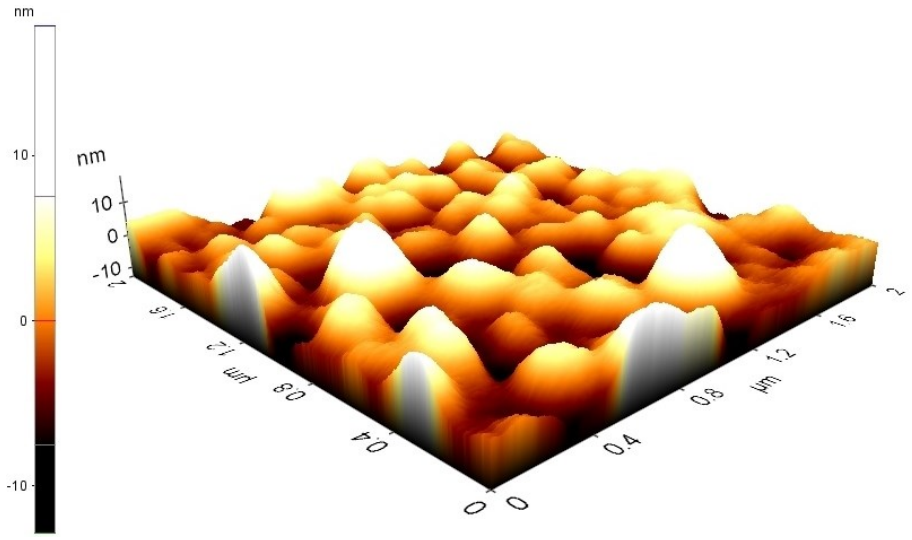

Figure B.1: The three dimensional surface map, over a 2 $\mu m \times 2\ \mu m$ silicon nitride covered titanium track of the uncoated MEA, as obtained from AFM.

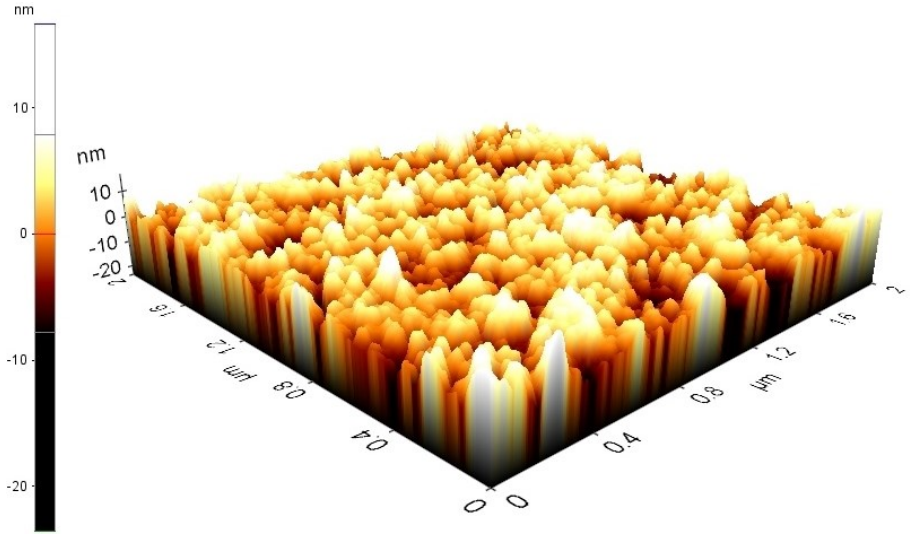

Figure B.2: A three dimensional surface map as acquired using AFM, over a 2 μm × 2 μm silicon nitride covered titanium track of the MEA coated with PEI.

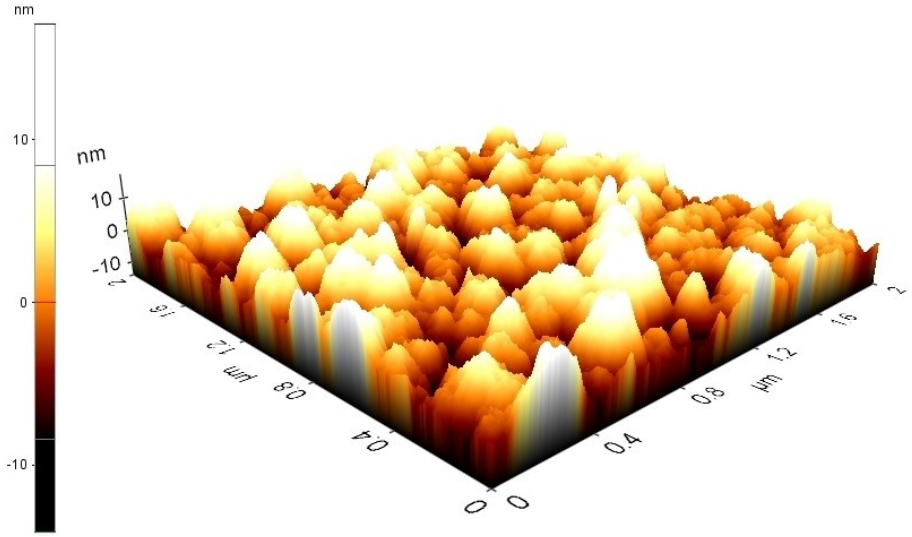

Figure B.3: The three dimensional surface map, over a 2 μm × 2 μm silicon nitride covered titanium track of the MEA coated with PEI and laminin.